Picosecond dynamics and photoisomerization of stilbene in supersonic beams. II. Reaction rates and potential energy surface

J. A. Syage, P. M. Felker,[a] and A. H. Zewail[b]
Arthur Amos Noyes Laboratory of Chemical Physics,[c] California Institute of Technology, Pasadena, California 91125

(Received 18 April 1984; accepted 3 July 1984)

Using picosecond excitation in a supersonic jet, we present a full account of our earlier report on the dynamics of state-selective photoisomerization of *t*-stilbene. Collisionless isomerization in this case indicates the twisting of the molecule about the ethylene bond away from the *trans* configuration

Central to this reaction is the question of vibrational energy redistribution or IVR. From direct (single vibronic level) time-resolved measurements, relative fluorescence quantum yields from relaxed and unrelaxed states, and a thorough vibrational analysis from excitation and dispersed fluorescence spectra (previous paper), the following conclusions are reached: (i) The IVR yield is state selective being more extensive from combination modes than from fundamental modes of similar energy. The IVR yield becomes very significant above $\approx$900–1000 cm^{-1}. The rate is much faster than the reaction at all energies studies. (ii) The barrier to isomerization is observed at 3.3 ± 0.2 kcal/mol (1100–1200 cm^{-1}). The radiative lifetimes, measured from the 0° level fluorescence decays, are 2.7 ± 0.1 ns (h_{12}) and 2.5 ± 0.1 ns (d_{12}). (iii) The observed isomerization rates in the isolated molecule are approximately an order of magnitude less than the calculated RRKM rates and observed solution phase rates. (iv) The apparent non-RRKM behavior in the isolated behavior is explained by considering the nature of IVR and by adopting a *diabatic* representation of the reactive surface (i.e., an allowed surface) using a Landau–Zener–Stueckelberg model. (v) Finally, we compare *t*-stilbene with other related isolated molecules and to solution phase *t*-stilbene results in order to assess the role of mode mixing and the nature of the reactive surface.

I. INTRODUCTION

The photoisomerization or reaction of any molecule under *collisionless* conditions requires a redistribution of energy from the initially excited mode to the reactive modes. The rate of this intramolecular vibrational redistribution (IVR) relative to the rate of reaction governs whether or not the reaction will be mode specific. In the preceding paper,[1] we undertook the first step towards understanding this problem in the collisionless photoisomerization of *trans*-stilbene by presenting a detailed vibrational analysis of the excited S_1 and ground S_0 electronic states of *t*-stilbene-h_{12} and -d_{12}. Spectral features which are particularly relevant to isomerization (e.g., low frequency torsions) and intermode couplings (e.g., Fermi resonances) were discussed in detail.

In this paper, we extend the vibrational details to consider dynamical effects in the reaction mechanism. These efforts rely on direct time-resolved measurements of the reaction rates from specific vibronic levels in S_1. (By reaction or isomerization, we mean the twisting of the molecule about the ethylene bond away from its initial *trans* configuration.[2]) We likewise, analyze spectral features which bear on the rate and extent of IVR from single vibronic levels (SVL). The experimental data are further analyzed under various theoretical models pertaining to isoenergetic rate processes in isolated molecules. By this approach we address some major points relating to intramolecular reaction dynamics such as;

(i) How does IVR relate to the observed reaction rates?

(ii) Are the IVR and reaction rates energy or mode dependent? If so, then how specific is this dependence?

(iii) What is the nature of the reactive surface? In terms of the postulated role of a surface crossing,[3] how does symmetry affect the avoidedness of the crossing and hence the adiabaticity of the reaction?

(iv) What is the nature of the torsional modes and how extensive is their coupling to other modes and to the reactive coordinate?

(v) What is the role of solvent and how does it affect the surface crossing and hence the barrier to isomerization?

Historically, the mechanism of *trans–cis* isomerization of stilbene has attracted much interest. The early spectroscopy of the S_1 state indicated that the ethylene bond order did not change significantly upon excitation.[4] On this basis, the S_1 barrier to isomerization should not be very different than in the ground state (46 kcal).[5] Photochemical studies, how-

[a] IBM Predoctoral Fellowship.
[b] Camille and Henry Dreyfus Foundation Teacher–Scholar.
[c] Contribution No. 7014.

 0021-9606/84/234706-18$02.10

ever, proved otherwise, with reported barriers ranging from 2–4 kcal.[4–9] Speculation as to the origin of this behavior has included consideration of a triplet mechanism and nonvertical excitation (for a review see Saltiel *et al.*, Ref. 5) The currently accepted explanation for the anomalously small barrier was proposed by Orlandi and Siebrand.[3] In this scheme, the barrier is the result of a curve crossing between the S_1 and a higher excited state surface that exhibits a minimum at the perpendicular configuration ($\vartheta = 90°$) of stilbene. The latter surface is known to be of A_g symmetry and in fact correlates with the ground S_0 surface with which it forms an avoided crossing at $\vartheta = 90°$.

A surface that illustrates the above features qualitatively and takes account of our findings is presented in Fig. 1. A number of theoretical[10,11] and (two-photon) experimental[11,12] studies have focused on the electronic states and the A_g surface that undergoes the crossing with S_1, however, questions remain regarding the ordering of the low lying A_g states.[11] Jet beam studies on the series of molecules styrene,[13] *t*-stilbene,[2,14] and diphenylbutadiene[15] indicate that the energy of the crossing decreases with increasing conjugation. However, whether the crossing is allowed or avoided (which determines whether the reaction proceeds diabatically or adiabatically, respectively) is still unresolved and represents an issue we address in this paper.

An interesting question regarding the reactive surface is: How do the dynamics of the molecule on the surface lead to isomerization under collision-free conditions? Time-resolved measurements of vapor phase *t*-stilbene have demonstrated that the lifetime varies with excess energy in the excited singlet state.[16] The molecules in these bulb experiments, however, carried thermal energy, which was much higher than the barrier height. Because of the thermal energy, the molecules could not be excited into specific vibronic states to address the issue of mode specificity. In our earlier report on *t*-stilbene in supersonic jet beams,[2] we obtained state-selective rates as a function of excess vibrational energy. In that study, the threshold to reaction in the isolated molecule was found to be $\approx 1200\ cm^{-1}$. The rate of IVR was also estimated and a model for isomerization following energy redistribution was proposed. In this manner it was concluded that IVR is much faster than reaction, a result supported by the absence of mode selectivity in the measured rate of isomerization. Subsequently, the relative quantum yields were measured as a function of excess energy by Amirav and Jortner[17] and Zwier *et al*[18] giving results in agreement with our picosecond/jet results.

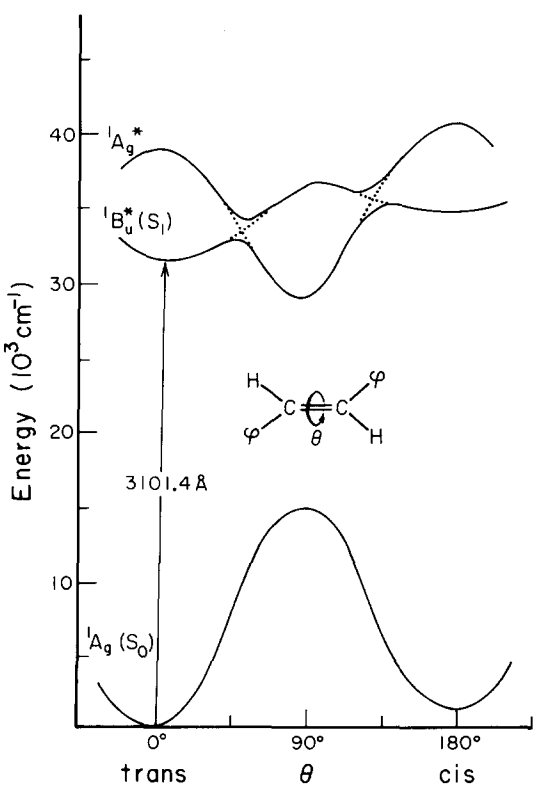

FIG. 1. Approximate potential energy diagram for the ground S_0 and the excited electronic states as a function of the ethylene torsional coordinate ϑ. The surface crossings are treated as adiabatic (avoided crossing;—) or diabatic (allowed crossing;···).

This paper, and the preceding one, extends the work of our earlier study[2] and addresses in greater detail the questions posed above. Future papers on stilbene isomerization will deal with direct time-resolved measurements of the energy dependent rate of IVR from recent pump–probe experiments in the beam[14] as well as the manifestations of quantum beats observed in the fluorescence decays from certain vibronic levels.

The present paper (II) is organized as follows: In Sec. II we report experimental details such as the picosecond laser/continuous jet apparatus, treatment of data and preparation of materials. In Sec. III we present the vibrational analysis relevant to isomerization (the details of which are given in the previous paper[1] I) and describe the results of our energy specific time-resolved measurements. A discussion of the single vibronic level reaction dynamics of *t*-stilbene is encompassed in Sec. IV. The section begins with a microscopic model for describing the kinetics of isomerization from specifically excited single vibronic levels (Sec. IV A). We then relate the IVR yield to the integrated fluorescence intensities from "relaxed" and "unrelaxed" vibrational levels in S_1 (Sec. IV B). Finally, the dynamics and nature of the reactive potential energy surface are discussed in terms of the effects of the electronic surface crossing on the rates of reaction (Secs. IV C and IV D). There we focus on models for the isoenergetic reaction mechanism by employing various rate expressions including RRKM and by investigating the role of entropy as it relates to the density of states in the reactant and product vibrational manifolds. The adiabaticity of the reactive trajectory is explored in terms of the degree of "avoidedness" of the surface crossing. We also compare our results both to solution phase studies to assess the role of the solvent and to other related molecules which undergo isomerization in order to better understand the excited state surfaces.

II. EXPERIMENTAL

The pulsed[19,20] and continuous supersonic jet[21] systems were briefly described in the preceding paper.[1] Complete details may be found in previous publications.[19–21] The picosecond laser/continuous jet system was used for all time-re-

solved data reported in this paper, hence we briefly discuss the essential details here.

A. Picosecond laser-continuous jet apparatus

The continuous jet apparatus is equipped with a 12 in. ring jet diffusion pump which maintains an ambient pressure of 10^{-4} Torr during normal operation. The jet is excited with a picosecond dye laser, synchronously pumped by a mode-locked argon ion laser. The dye pulses were cavity dumped (variable from 0.8 to 4 MHz) and frequency doubled with $LiIO_3$ to give UV pulses with temporal and frequency pulse widths (FWHM) of ≈ 15 ps and ≈ 0.3 Å, respectively.

The fluorescence was collected using $f/1$ optics and imaged onto a microprocessor controlled 0.5 m monochromator. Spectra were recorded by time-correlated single-photon counting using a fast photomultipler and a time-to-amplitude converter (TAC). This technique relies on converting the time that a photon is emitted after laser excitation to a voltage signal via a voltage ramp generated by the TAC. All data were collected on a multichannel analyzer and transferred to a PDP 11/23 computer. (For more details see Ref. 21.)

The trans-stilbene-h_{12} or -d_{12} was heated to ≈ 100 °C and expanded through a 150 μm pinhole. All expansions in the continuous jet were backed by ≈ 35 psi He unless otherwise noted. Excitation of the jet cooled molecules by the picosecond pulses occurred 5 mm from the nozzle. No change in the fluorescence decay times was observed at longer distances indicating that collision-free conditions were effectively achieved.

B. Treatment of data

The picosecond decay curves were deconvoluted using an iterative nonlinear least squares algorithm. The temporal response function of the system was obtained by recording the response of the laser pulse by scattering it off the nozzle. The quality of the exponential fits was uniformly excellent as judged by the reduced χ^2 values and the weighed residuals which display the point-by-point deviations of the experimental curve from the fitted curve. The data presented here represent an average over many determinations and are reported with their standard deviation.

C. Materials

The *t*-stilbene-h_{12} (Aldrich, 96%) was recrystallized in absolute ethanol. The purity of the material before and after recrystallization was determined by gas chromotography to be 97.5% and 99 + %, respectively. The *t*-stilbene-d_{12} was obtained from Merck (98% d atom) and used as is.

III. RESULTS

A. Spectra: Important features below and above the reaction barrier

A detailed vibrational analysis of the S_0 and S_1 states of *t*-stilbene-h_{12} and -d_{12} is reported in the preceding paper.[1] Here we present results pertinent to the isomerization process. The excitation spectrum of *t*-stilbene-h_{12} is illustrated from 3101.4 Å (0 cm^{-1}) to ≈ 2775 Å (3400 cm^{-1}) in Fig. 2.

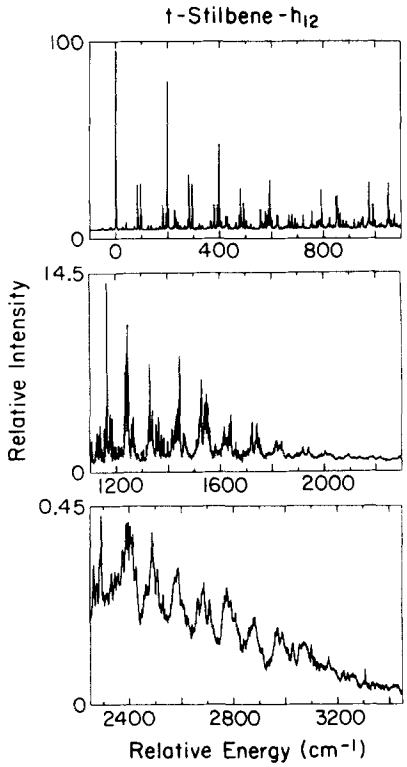

FIG. 2. Fluorescence excitation spectra of *t*-stilbene-h_{12} for $^1B_u \leftarrow {}^1A_g$ electronic excitation. Recorded using the pulsed jet system under expansion conditions of 50 psi He and 80 °C sample temperature. These spectra have been adapted from the previous paper (Ref. 1).

The corresponding spectrum of the -d_{12} isotope is given in the preceding paper. In Table I we have compiled the vibrational modes of the S_0 and S_1 states that are relevant to our discussion of the dynamics.

Certain qualitative features in the excitation spectra of *t*-stilbene deserve comment. A sharp decrease in band intensities is observed for vibrational energies greater than 1500 cm^{-1}. This is attributed to isomerization which competes with radiative decay as discussed in the coming sections and in our earlier report.[2] Time-resolved measurements indicate that the barrier (for -h_{12}) for isomerization occurs at about 1100–1200 cm^{-1} (Figs. 3 and 4), however, the rate of isomerization in the near vicinity of the barrier is not rapid enough to effectively quench the fluorescence as it does at higher energies. A previous study on the jet-cooled excitation spectra of *t*-stilbene[17] has reported that the spectrum becomes continuous at excess energies E_x greater than 1500 cm^{-1}. However, it is clear in Fig. 2 that sharp features are still discernable at energies well in excess of 2000 cm^{-1}, although a broad background due to spectral congestion does emerge.

The dispersed fluorescence spectra recorded from single vibronic level (SVL) excitation enables one to examine qualitatively (but not prove) the onset and extent of intramolecular vibrational redistribution (IVR) especially in the statistical limit. IVR plays a crucial role in isomerization (or any reaction involving discrete excitation) in that it is the mechanism by which the energy of the initially excited mode flows into the reactive modes.

The detailed SVL dispersed fluorescence spectra for *t*-stilbene-h_{12} and -d_{12} appear in the preceding paper.[1] We

TABLE I. Assignment of the totally symmetric (a_g) S_1 and S_0 vibrations of *t*-stilbene.

Symmetry and mode no.[a]		Approximate description	S_1 state		S_0 state	
			h_{12}	d_{12}	h_{12}	d_{12}
1	[20*b*]	CH st				
2	[7*b*]	CH st				
3	[2]	CH st				
4	[13]	CH st				
5	[20*a*]	CH st (C_e sens)				
6		C_eH st				
7		C_eC_e st	1637.8?	1579.0?	1654	1613
8	[8*a*]	CC st	1553.0?	1522.4?	1607	1573
9	[8*b*]	CC st	1548.4	1504.3	1584?	1549?
10	[19*a*]	CC st	1463–66?	...	1495?	1351, 1380?
11	[19*b*]	CC st + CCH ben	1429.7?	1306.7?	...	...
12	[14]	CCH ben + CC st	1332.4	...	1340	...
13		C_eC_eH ben	1249.3	989.6?	1321	1023
14	[3]	CCH ben	1264.2?	969.6?	...	...
15	[13]	$C_e\varphi$ st	1170.3?	1125.0	1208	1152
16	[9*a*]	CCH ben	...	859.0?	1188	872
17	[15]	CCH ben	...	866.8?	1162?	...
18	[18*b*]	CCH ben	1069.8?	778.3	1072	828?
19	[18*a*]	CCH ben	994.9	741.3	1026	786
20	[12]	CCH ben + CC st + CCC ben	972.7	934.3	1006	962
21	[1]	$C_eC_e\varphi$ ben + CCC ben	845.8–851.9	829.5?	870	847?
22	[6*a*]	CCC ben (C_e sens)	621.7	579.9	646	610
23	[6*b*]	CCC ben	590.7	565.6	624	592
24	[9*b*]	C_eCC ben	280.3	263.7	290	272
25		$C_eC_e\varphi$ ben	197.6	187.9	204	191

[a] Symmetry elements are for C_{2h} symmetry. Mode designations in brackets [ ] refer to benzene type modes according to Varsanyi's convention (Ref. 50).

present some spectra in later sections (cf. Figs. 10–14) as they pertain to the question of IVR. We have denoted the vibronic excitation and emission bands as A_n^m, where A is the mode number (cf. Table I) and n and m are the number of quanta of mode A in the S_0 and S_1 electronic states. Combination bands are therefore expressed as $A_n^m B_{n'}^{m'} \cdots$ and excited state SVLs as $A^m B^{m'} \cdots$.

In Sec. IV, we describe a microscopic kinetic model for IVR and reaction which relates the rate of IVR to the integrated intensity of the "relaxed" and "unrelaxed" fluorescence and to the density of states. However, we remark on a

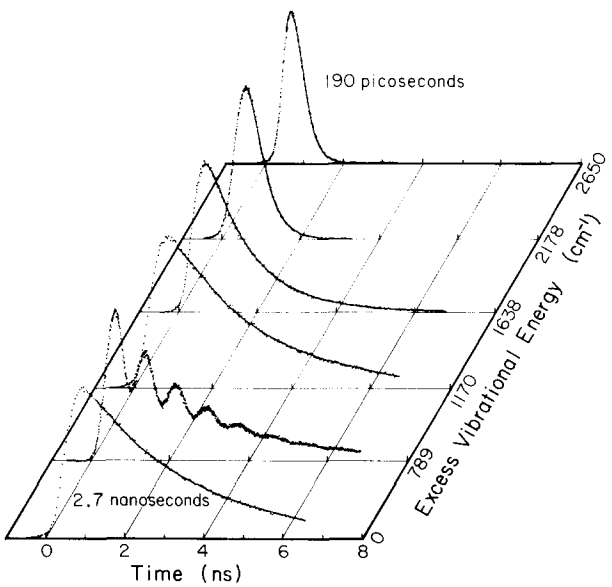

FIG. 3. Observed time-resolved decay curves for *t*-stilbene-h_{12} for various SVL vibrational energies in S_1.

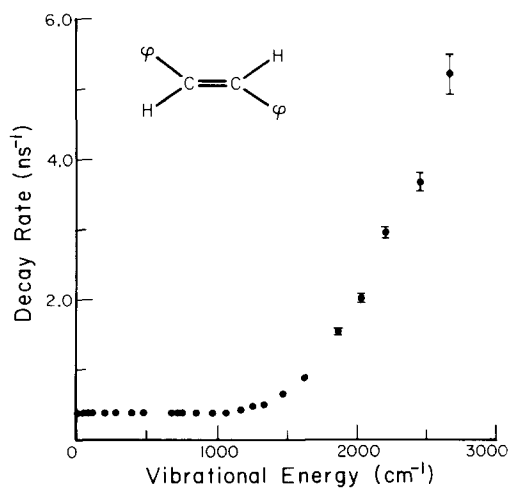

FIG. 4. Observed fluorescence decay rates for *t*-stilbene-h_{12} as a function of vibrational energy in S_1. Error bars represent standard deviations. The absence of error bars indicates that the standard deviation is smaller than the point size.

few qualitative observations of the SVL fluorescence spectra presented in Sec. IV B. Most obvious is the emergence of a broad continuum-like fluorescence which increases with vibrational energy E_x. The broadening occurs since the fluorescence spectra from the redistributed modes generally differ from the spectrum of the initially excited SVL. Because the rate and extent of IVR is expected to depend on the density of the accepting modes at E_x and the coupling strength between the initial mode and the accepting modes, it is plausible to relate the broadening to the extent of IVR. Caution, however, must be taken to insure that the broadening is not due to spectral congestion and instrument (e.g., spectrometer) resolution. With this in mind one concludes that an apparent onset for IVR occurs at $E_x \approx 900$–1000 cm^{-1}, however, a state-selective acceleration of yield occurs below this energy (see Table II and Fig. 8). The direct time-resolved measurement of IVR using pump–probe techniques are now in progress and will be dealt with elsewhere.[14]

B. Time-resolved spectra

Direct measurements of the fluorescence decay following SVL excitation were recorded with the picosecond/jet apparatus. Preliminary results for *t*-stilbene-h_{12} were reported in our earlier study[2] which we supplement here with additional and more refined data. The results for the -d_{12} labeled compound are presented for the first time. Examples of decay curves for various vibrational energies E_x are illustrated in Fig. 3 along with the iterative fits. The time-resolved spectra exhibit clean single exponential decays. There is, however, indication of a second component at certain excess energies where quantum beats are observed. These beats, similar to those found in anthracene,[21–23] are observed below the barrier to isomerization and will be dealt with in a separate publication.[24] As shown by Felker and Zewail,[23] quantum beats can be directly related to the process of restricted IVR. We show a typical example of a beat modulated fluorescence decay spectrum in Fig. 3. These observations of

TABLE II. Calculated yields and rates of IVR from relative fluorescence quantum yield measurements.[a]

Energy (cm^{-1})	Assignment	Φ_{IVR}[b]	k_{IVR}/α (ns^{-1})[c]
166	2×83	0.67	0.75
198	ν_{25}	0.21	0.10
376	$83+95+198$	0.76	1.2
396	2×198	0.55	0.45
472	$2\times95+83+198$	0.89	2.9
591	$\nu_{23}[\nu_{6b}]$	0.26	0.13
592	3×198	0.65	0.70
622	$\nu_{22}[\nu_{6a}]$	0.27	0.14
663	oop[d]	0.71	0.90
675	$280+2\times198$	0.90	3.5
687	$591+95$, $3\times198+95$	0.79	1.4
717	oop[c]	0.64	0.65
789	$591+198$	0.69	0.81
821	$622+198$	0.87	2.5
846	$\nu_{21}[\nu_1]$	0.60	0.55
849	Fermi resonance	0.71	0.89
852		0.84	2.0
873	$83+591+198$	0.96	8.1
973	$\nu_{20}[\nu_{12}]$	0.81	1.6
987	$591+2\times198$	0.93	4.8
995	$\nu_{19}[\nu_{18a}]$	0.79	1.4
1045	$849+198$	0.82	1.7
1048	$852+198$	0.92	4.4
1070	$83+591+2\times198$, $\nu_{18}[\nu_{18b}]$?	0.98	19.1
1170	$973+198$, $\nu_{15}[\nu_{13}]$?	0.98	17.5

[a] Φ_{IVR} and k_{IVR} are determined from Eqs. (14) and (15).
[b] We consider the primary source of error to be in distinguishing sharp from broad fluorescence. The uncertainty in determining $(1-\Phi_{IVR})$ is about 10%–20% and that for k_{IVR} about 20%–30%.
[c] This assumes that k_{IVR} approximates an exponential rate constant (see the text).
[d] Out-of-plane fundamental.

TABLE III. Measured rates of fluoresence decay following state-selective vibronic excitation in *t*-stilbene.

Vibrational energy (cm^{-1})[a]	τ_f(ns)[b]	k_{fl}(ns^{-1})[b,c]	k_{nr}(ns^{-1})[d]
$-h_{12}$			
0	2.67 ± 0.03	0.374 ± 0.004	...
39	2.56	0.391	0.017
83	2.59	0.386	0.012
95	2.59	0.386	0.012
198	2.65 ± 0.05	0.378 ± 0.007	0.004
280	2.61	0.383	0.009
396	2.60 ± 0.05	0.385 ± 0.008	0.011
478	2.55	0.392	0.018
675	2.65	0.377	0.003
717	2.59	0.386	0.012
752	2.65 ± 0.08	0.378 ± 0.012	0.004
849	2.63 ± 0.03	0.380 ± 0.004	0.006
973	2.60 ± 0.03	0.385 ± 0.004	0.011
1048	2.68 ± 0.06	0.374 ± 0.008	...
1170	2.33 ± 0.03	0.429 ± 0.006	0.055
1246	2.01	0.498	0.124
1332	1.94 ± 0.06	0.515 ± 0.016	0.141
1447	1.50 ± 0.08	0.667 ± 0.035	0.293
1638	1.11 ± 0.10	0.906 ± 0.083	0.532
1839	0.64 ± 0.04	1.56 ± 0.10	1.19
2011	0.49 ± 0.03	2.04 ± 0.10	1.66
2178	0.34 ± 0.01	2.98 ± 0.08	2.61
2429	0.27 ± 0.01	3.69 ± 0.19	3.32
2650	0.19 ± 0.02	5.26 ± 0.5	4.89
$-d_{12}$			
0	2.53 ± 0.06	0.395 ± 0.010	...
36	2.50	0.400	0.005
76	2.50	0.400	0.005
87	2.52	0.397	0.002
188	2.58	0.388	...
376	2.53	0.395	...
527	2.51	0.398	0.003
754	2.48	0.403	0.008
830	2.42	0.413	0.018
859	2.43	0.411	0.016
934	2.44 ± 0.02	0.411 ± 0.003	0.016
990	2.42	0.413	0.018
1078	2.40	0.417	0.022

[a] The assignments of these states may be found in Table II or in Ref. 1.
[b] Error limits represent standard deviations for all measurements taken at each energy. Data without error limits represent one determination. The systematic error (not included above) is estimated to be about 50 ps.
[c] The measured fluorescence decay rate corresponds to decay from $|s\rangle$ and $\{|l\rangle\}$ below the isomerization threshold at $\approx 1200\ cm^{-1}$. Above this energy, $k_{fl}=\lambda_l$; cf. Eq. (11).
[d] The nonradiative rate constant k_{nr} is determined by taking $k_{rad}=k_{fl}$ at the 0^0 level.

quantum beats require resolved fluorescence detection, otherwise the modulation can "wash out".[23] The decay curves illustrated in Fig. 3 were recorded using single band fluorescence detection. At excess energies where no modulation was observed, the decay times for different fluorescence bands were the same, hence, some of the data (e.g., above the reaction barrier) were obtained from broadband fluorescence decay spectra. All time-resolved spectra are observed to decay to the baseline, hence the presence of a long time component can be no greater than the baseline uncertainty (i.e., <0.01).

The experimentally determined decay rates are plotted as a function of vibrational energy for *t*-stilbene-h_{12} in Fig. 4 and compiled for both h_{12} and d_{12} compounds in Table III. The 0^0 level lifetime was measured to be 2.7 ± 0.1 ns (h_{12}) and 2.5 ± 0.1 ns (d_{12}). These times are longer than previous determinations in either the solution or vapor phase.[7,8,16,25,26] The estimated radiative lifetime in solution is 1.7 ns[6,25] and hence our result may be considered to be a better estimate of the true radiative lifetime in the *isolated* molecule. It should be mentioned that in solution, a correction for the refractive index of the solvent is necessary to obtain the true radiative lifetime.[27]

IV. ANALYSIS AND DISCUSSION

A. The dynamics of isomerization

1. Model for collisionless isomerization

The kinetics following laser excitation of molecules in supersonic beams differ from conventional thermal reactions in two fundamental ways: (i) single vibrational levels in the excited electronic state may be excited in jet-cooled molecules; and (ii) the molecules are collision free and hence subject to intramolecular interactions only. A system of isolated, isoenergetic molecules (i.e., a microcanonical ensemble) that undergoes reaction requires a microscopic rate theory to describe the kinetics from specifically prepared vibrational states. The model we shall adopt here is the following: the laser excites a pure state $|s\rangle$ which redistributes the energy (by IVR) to a manifold of states $\{|l\rangle\}$. The $\{|l\rangle\}$ states undergo the photochemical change along the twisting coordinate (i.e., reaction coordinate) to form product or $\{|p\rangle\}$ states. If the rate of IVR is much faster than the reaction rates, then the latter will be mode independent.

The quantum mechanical solution to a similar problem has been worked out in the context of radiationless transition theory.[28] A kinetic model can be adopted provided the correspondence between the two descriptions is made.[28] As discussed in Ref. 19, if coherence (e.g., quantum beats) among levels is not present, then this correspondence is more adequate because we do not have to be concerned with the quantum mechanical interference that a kinetic model ignores. The quantum mechanical model, under the usual approximations, predicts biexponential decay; the fast component due to the dephasing of the levels and the long component due to the decay of the interacting (or mixed $|s\rangle$ and $\{|l\rangle\}$) states. The corresponding behavior in the kinetic model associates the fast component to the equilibration of $|s\rangle$ and $\{|l\rangle\}$, and the long component to the decay of the equilibrated states. According to this model, the kinetics for the populations N of these states may be described by

$$N_s = -(k_{sg} + k_{sl})N_s + k_{ls}N_l, \tag{1}$$

$$N_l = -(k_{lg} + k_{ls} + k_{lp})N_l + k_{sl}N_s + k_{pl}N_p, \tag{2}$$

$$N_p = -(k_{pg} + k_{pl})N_p + k_{lp}N_l, \tag{3}$$

where the rate constants are defined in Fig. 5.

2. Application to time-resolved fluorescence

Equations (1)–(3) do not have simple analytic solutions. In the following we discuss conditions under which the solutions of the coupled rate equtions simplify. In particular, we show that the kinetic scheme (Fig. 5) may be decoupled to a three state problem described by

$$\{|a\rangle\} \underset{k_{ba}}{\overset{k_{ab}}{\rightleftharpoons}} \{|b\rangle\}$$

$$k_{ag} \searrow \quad \swarrow k_{bg},$$

$$\{|g\rangle\}$$

where the pair of subset states $\{|a\rangle\}, \{|b\rangle\}$ represents either $|s\rangle, \{|l\rangle\}$ or $\{|l\rangle\}, \{|p\rangle\}$ depending on the cases discussed below. The solution of the above scheme is general in both cases and is given by

$$I_a(t) = k^r_{ag} K\{e^{-\lambda_a t} + me^{-\lambda_b t}\}N_a(0), \tag{4}$$

$$I_b(t) = k^r_{bg} F\{e^{-\lambda_b t} - e^{-\lambda_a t}\}N_b(0), \tag{5}$$

$$K = \frac{\Lambda_a - \lambda_b}{\lambda_a - \lambda_b}, \quad F = \frac{k_{ab}}{\lambda_a - \lambda_b}, \tag{6a}$$

$$m = \frac{\lambda_a - \Lambda_a}{\Lambda_a - \lambda_b}, \tag{6b}$$

$$\Lambda_a = k_{ag} + k_{ab}, \tag{6c}$$

$$\Lambda_b = k_{bg} + k_{ba}, \tag{6d}$$

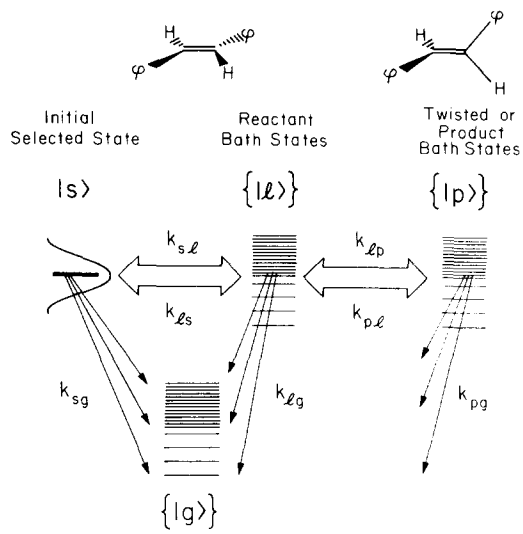

FIG. 5. Microscopic kinetic representation for SVL excitation in isolated molecules. The rate constant k_{sl} represents the rate of IVR to the subset of states $\{|l\rangle\}$ encompassed within the excitation bandwidth of $|s\rangle$. The *t*-stilbene reaction along an excited electronic surface involves the conversion from a planar to a perpendicular geometry. The model allows for reversibility of IVR and reaction as indicated by the double arrows. Decay to the ground state, however, is considered to be irreversible.

$$\lambda_{a,b} = \tfrac{1}{2}\{(\Lambda_a + \Lambda_b) \pm [(\Lambda_a - \Lambda_b)^2 + 4k_{ab}k_{ba}]^{1/2}\}, \quad (6e)$$

where we have expressed the state populations in terms of the fluorescence intensity by the simple relation

$$I_a = k^r_{ag} N_a, \quad (7)$$

where k^r_{ag} is the radiative rate constant. We mention that the rate constants to the ground state $|g\rangle$ have been expressed as a sum of radiative and nonradiative terms in Eqs. (6c) and (6d). Actually, the states within the subset $\{|l\rangle\}$ may have different decay rates, however, due to equilibration or similar Franck–Condon factors we assume that they are very similar. This is consistent with the resolved fluorescence lifetimes which do not change with wavelength for a given excitation energy.

With the discussion of Sec. IV A1 in mind, we may relate the forward and backward rate constants to the density of states as follows:

$$\frac{k_{ab}}{k_{ba}} = \frac{\rho_b}{\rho_a} \quad (8)$$

implying that for the $s \leftrightarrow l$ process, the forward rate is always greater than the reverse rate. Hence, the concept of an irreversible heat sink emerges depending on this ratio (which is different for stilbene below and above the reaction barrier).

a. Below the reaction barrier $k_{lp} = 0$. In the absence of reaction, N_p decouples from the rate equations in Eqs. (1)–(3) and the solution reduces to the form given by Eqs. (4)–(6). Here $|a\rangle$ and $|b\rangle$ are associated with the initially excited SVL $|s\rangle$ and the bath states $\{|l\rangle\}$, respectively.

The rate constant k_{sl} should be recognized as the rate constant for IVR. Equations (4) and (5) indicate that the decay of $|s\rangle$ and formation of $\{|l\rangle\}$ is biexponential. This behavior is a consequence of the return channel k_{ls}. However, according to Eq. (8), as the density of states ρ_l increases, the subset of states $\{|l\rangle\}$ takes on the characteristics of an irreversible heat bath. In the limit where $\rho_l/\rho_s \gg 1$, it may be shown that Eqs. (4) and (5) reduce to the simple form

$$I_s(t) = k^r_{sg} e^{-\Lambda_s t} N_s(0), \quad (9)$$

$$I_l(t) = k^r_{lg} F\{e^{-\Lambda_l t} - e^{-\Lambda_s t}\} N_s(0), \quad (10)$$

where we have expressed the generalized states a and b in terms of s and l, and Λ_s and Λ_l are given in Eq. (6). Note that when IVR is absent, the decay of $|s\rangle$ is given simply by k_{sg} and $F \to 0$. When IVR is present, but not extensive, a biexponential decay is predicted [Eq. (4)]. This biexponential behavior has recently been observed in the unrelaxed fluorescence region of anthracene.[23]

The rates of IVR k_{sl} in stilbene at high energies are typically very fast as measured recently.[14] However, it is possible to obtain estimates of k_{sl} from the integrated fluorescence intensity of the unrelaxed (from $|s\rangle$) and relaxed (from $|l\rangle$) fluorescence. (We derive the expressions very shortly in Sec. IV A 3).

b. Above the reaction barrier $k_{lp} \neq 0$. By coupling into the product states $\{|p\rangle\}$, the solution of Eqs. (1)–(3) becomes tedious. However, if we again invoke the intermediate to large density of states condition $\rho_l/\rho_s \gg 1$, then we may effectively decouple the initial state $|s\rangle$ from the rate equations.

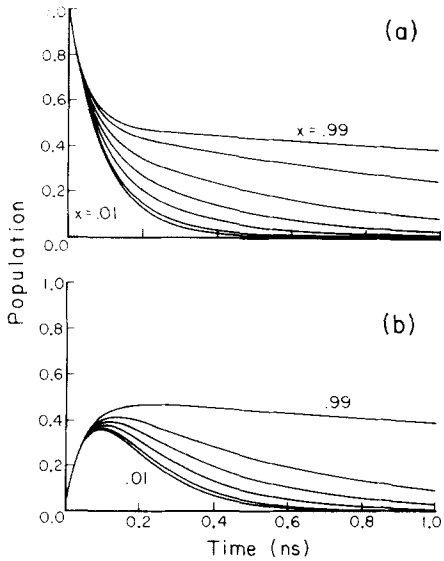

FIG. 6 Calculated time dependence of (a) $\{|l\rangle\}$ and (b) $\{|p\rangle\}$ for $\Lambda_p \approx \Lambda_l$. Input parameters for Λ_l were $k_{lp} = 1\times10^{10}$ s^{-1} and $k_{lg} = k^r_{lg} = 4\times10^8$ s^{-1}. Parameters for Λ_p were $k_{pl} = x\Lambda_p$ where $\Lambda_p = k_{pl} + k_{pg} = 1\times10^{10}$ s^{-1}. Calculated curves are for values $x = 0.99$, 0.90, 0.70, 0.50, 0.30, 0.10, 0.01, from top to bottom.

This assumes that the rate of IVR k_{sl} is much faster than all other relevant processes so that the subset $\{|l\rangle\}$ may be treated as the initial state(s). The kinetic scheme for $\{|l\rangle\}$ and $\{|p\rangle\}$ now reduces to the simple form described above and may likewise be expressed by Eqs. (4)–(6), where instead $|a\rangle = \{|l\rangle\}$ and $|b\rangle = \{|p\rangle\}$. Naturally, if quantum beats are observed (indicating restricted IVR) then this approximation is not as valid (Sec. IV A 1).

In time-resolved fluorescence experiments one is usually concerned with the detection of $\{|l\rangle\}$ since the product states $\{|p\rangle\}$ often do not fluoresce. Equation (4) indicates that the decay properties are described by a double exponential function. This behavior is illustrated in Fig. 6 for $\{|l\rangle\}$ and $\{|p\rangle\}$ in the case where the total decay constants from the two sets of states are similar (i.e., $\Lambda_a \approx \Lambda_b$). If the rate of decay from $\{|p\rangle\}$ should increase in relation to $\{|l\rangle\}$, the steady state population of $\{|p\rangle\}$ will decrease. Consequently, the first decay component in $\{|l\rangle\}$ will likewise diminish in importance. This property is evident in Fig. 7(a) where the calculated curves for $\Lambda_b = 10\Lambda_a$, exhibit nearly single-exponential decay from $\{|l\rangle\}$.

We consider expressions for the simple and fairly common situation where $\{|p\rangle\}$ decays (other than by reversing to $\{|l\rangle\}$) much faster than $\{|l\rangle\}$ since this leads to single exponential decays for $\{|l\rangle\}$ in agreement with our experimental results. This situation is represented by the condition $\Lambda_b \gg \Lambda_a$ [Eqs. (6c)(6d)]. It then follows from Eq. (6e) that $k_{lp}k_{pl} \ll (\Lambda_a - \Lambda_b)^2$ and therefore $\lambda_b \gg \lambda_a$. Equation (4) then reduces to

$$I_l(t) = k^r_{lg} e^{-\lambda_l t} N_l(0), \quad (11a)$$

$$\lambda_l \approx \Lambda_l - \frac{k_{lp}k_{pl}}{\Lambda_p} = k_{lg} + k_{lp}\left(1 - \frac{k_{pl}}{\Lambda_p}\right), \quad (11b)$$

where we have explicitly denoted a and b as l and p, respec-

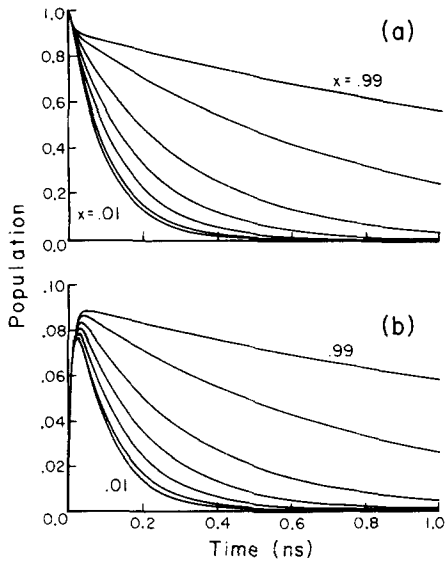

FIG. 7. Calculated time dependence of (a) $\{|l\rangle\}$ and (b) $\{|p\rangle\}$ for $\Lambda_p \approx 10\Lambda_l$. Input parameters are the same as in Fig. 7 except that $\Lambda_p = 1\times10^{11}\ s^{-1}$. Note the change of population scale for (b).

tively. The decay constant λ_l in Eq. (11b) was obtained by using the relations above and factoring the square root term[29] in Eq. (6e).

Equation (11) has very important consequences when measuring the forward rate constant for reaction k_{lp} by time-resolved fluorescence detection. When the principal decay process from $\{|p\rangle\}$ is decay to the ground state, k_{pg} (i.e., $k_{pl} \ll \Lambda_p$), then the measured decay constant λ_l leads *directly* to the reaction rate k_{lp} when account is taken of the radiative and nonradiative constant k_{lg}. On the other hand, as the back reaction k_{pl} contributes increasingly to the decay Λ_p of $\{|p\rangle\}$, the importance of the reaction rate constant k_{lp} on the measured decay constant λ_l diminishes. The decay curves in Figs. 6 and 7 were calculated for a fixed value of the forward rate constant k_{lp} and for the total decay rate Λ_p from $\{|p\rangle\}$; only the rate constants comprising Λ_p were varied. The application of this analysis to the experimental data is discussed in Sec. IV C 3.

We mention that one may obtain simple analytic expressions that consider both the rate of IVR k_{sl} and the rate of reaction k_{lp} if one assumes irreversibility for the two processes (i.e., $k_{ls} = k_{pl} = 0$). This approach was used in our previous paper[2] to describe *t*-stilbene isomerization from SVL excitation and to obtain estimates of the rate of IVR from SVL dispersed fluorescence spectra.

3. Integrated fluorescence intensity: Yield of IVR.

At this point we are concerned with the fluorescence from the unrelaxed $|s\rangle$ and relaxed states $\{|l\rangle\}$. Consequently, we associate *a* and *b* in Eqs. (4) and (5) with *s* and *l* and assume no reaction (i.e., $k_{lp} = 0$). Integrating over all time leads to expressions for the absolute quantum yield for fluorescence:

$$\Phi_s = \frac{1}{N_s(0)}\int_0^\infty I_s(t)dt = K_{sg}^r K\left[\frac{\lambda_l + m\lambda_s}{\lambda_s\lambda_l}\right], \tag{12a}$$

$$\Phi_l = \frac{1}{N_s(0)}\int_0^\infty I_l(t)dt = K_{lg}^r F\left[\frac{\lambda_s - \lambda_l}{\lambda_s\lambda_l}\right], \tag{12b}$$

where K and F are defined in Eq. (6a). The relative quantum yield expression is obtained by dividing Eqs. (12a) and (12b) to give

$$\frac{\Phi_l}{\Phi_s} = \frac{\int_0^\infty I_l(t)dt}{\int_0^\infty I_s(t)dt} = \frac{K_{lg}^r F}{K_{sg}^r K}\left[\frac{\lambda_s - \lambda_l}{\lambda_l + m\lambda_s}\right]. \tag{13}$$

Equation (13) is a particularly useful expression since it dispenses with the necessity of determining the number of molecules $N_s(0)$ initially excited. If we consider further the reasonable case discussed above where $\rho_l/\rho_s \gg 1$ (i.e., the intermediate/large density of states), then Eq. (13) simplifies considerably to

$$\frac{\Phi_l}{\Phi_s} = \frac{k_{lg}^r k_{sl}}{k_{sg}^r \Lambda_l}, \tag{14}$$

where now Λ_l is the experimentally measurable fluorescence decay rate from $\{|l\rangle\}$. Equation (14) is important because it relates the "rate" of IVR k_{sl} to experimentally determinable parameters. Since all the fluorescence presumably arises from the same electronic state, the ratio of the radiative rate contants k_{lg}^r/k_{sg}^r can be taken to be approximately unity. There are some uncertainties, however, in applying Eq. (14), such as differences in Franck–Condon factors between $|s\rangle$ and $\{|l\rangle\}$, as well as difficulties in distinguishing relaxed fluorescence from spectrally congested fluorescence.

Finally, Eq. (14) become less valid if k_{sl} is not an exponential decay constant [i.e., if it is a function of time, $k_{sl}(t)$]. Since the rate of IVR is dependent on the overlap of $|s\rangle$ with $\{|l\rangle\}$, it may be argued that IVR is favored at very early times possibly due to the contribution of uncertainty broadening to the overlap.[30] Under these conditions it is more correct to define a quantum yield for IVR $\Phi_{\rm IVR}$ which is given simply by

$$\Phi_{\rm IVR} = \frac{\alpha\Phi_l}{\alpha\Phi_l + \Phi_s}, \tag{15}$$

where $\alpha = k_{sg}^r/k_{lg}^r$.

B. State-selective IVR

The process of IVR is assumed here to be a prerequisite to isomerization. Clearly, if an unreactive vibronic state is excited, a redistribution of energy must occur to populate the reactive states. If the rate of IVR among all modes is much faster than reaction, it is commonly accepted that (on the average) the reaction will not exhibit any state selectivity. However, if IVR restricts the reaction rate then a state selectivity in the rate of IVR may be imparted to the reaction. There are reasons to expect such behavior in isolated molecules (although not necessarily at reactive energies). The rate of IVR is proportional to the effective density of states. However, the density of states is not generally a smoothly varying property, but can be rather coarse with pockets of dense and sparse level structures. Furthermore, the coupling between

the initially excited levels and the bath states may vary widely, thus giving rise to a state-selective rate of IVR. For instance, a restricted IVR was observed recently in anthracene by Felker and Zewail[23] at excess energies of $\approx 1500\ \mathrm{cm}^{-1}$ and also in stilbene below the barrier for isomerization (cf. Fig. 3).[24]

The rate constant for IVR k_{IVR} (i.e., k_{sl}, Fig. 5), was related to the relative quantum yields for unrelaxed and relaxed fluorescence in Eq. (14). However, it was noted that when k_{IVR} is not an exponential decay constant. IVR is best described in terms of a quantum yield Φ_{IVR} according to Eq. (15). The relation between k_{IVR} and Φ_{IVR} may be shown to be

$$k_{\mathrm{IVR}} = k_{sl} = \frac{\alpha \Lambda_l \Phi_{\mathrm{IVR}}}{1 - \Phi_{\mathrm{IVR}}} = \alpha \frac{\Phi_l}{\Phi_s} \Lambda_l, \tag{16}$$

where $\alpha = k^r_{sg}/k^r_{lg}$. We described Λ_l in Sec. IV A 3 as the experimentally measurable fluorescence decay rate from $\{|l\rangle\}$. The actual fluorescence decay, however, is a superposition of the decays from $|s\rangle$ and $\{|l\rangle\}$. The individual contributions to the decay may be distinguished from each other by collecting either unrelaxed (sharp) or relaxed (broad) fluorescence. For excitation energies in *t*-stilbene where unrelaxed fluorescence can still be detected (i.e., below the barrier to isomerization), the measured fluorescence decay constants Λ_s and Λ_l are equal. The rates are also essentially constant with energy up to the isomerization threshold (Fig. 4) and equal to the 0^0 level value which we have used to approximate the radiative rate constant k^r_{sg}. These arguments suggest (but do not prove) that $k^r_{lg} \approx k^r_{sg}$ (i.e., $\alpha \approx 1$) in which case, k_{IVR} or Φ_{IVR} can be determined from the experiments reported here.

We have thus far assumed that k_{IVR} is time independent. If this is the case, then the temporal behavior of the $|s\rangle$ and $\{|l\rangle\}$ states should be different if IVR occurs from $|s\rangle$ to $\{|l\rangle\}$ [Eqs. (9) and (10)]. On the other hand, if k_{IVR} is time dependent [ie., $k_{\mathrm{IVR}}(t)$] then it is possible for IVR to occur at early times, but not to completion. In this case, two experimental observations may occur: (i) the emission from $|s\rangle$ (sharp) and $\{|l\rangle\}$ (broad) may be distinguished, and (ii) if the time resolution is not sufficient to detect the IVR, then the measured decay from $|s\rangle$ and $\{|l\rangle\}$ below the reaction barrier may be similar, since only decay to the ground state $|g\rangle$ would be observed. Below the reaction barrier, we were able to distinguish both broad (relaxed) and sharp (unrelaxed) fluoescence and found that the decay times are very similar. This is consistent with a time dependent rate of IVR and may possibly have bearing on theoretical predictions[30] that IVR should be accelerated at early times due to uncertainty broadening. If IVR goes essentially to completion (e.g., above the reaction barrier), then the $\{|l\rangle\}$ states would be predominantly observed and hence the time dependence of k_{IVR} would not be a major concern.

We take a cautious stance in reporting values of Φ_{IVR} and k_{IVR} since a number of experimental complications come into play in using Eqs. (15) and (16). The most serious problem is broadening introduced by spectral congestion and the instrumental (e.g., monochromator) resolution. Here, we express k_{IVR} in terms of α. Although, the latter term has been specifically defined above, we may consider it

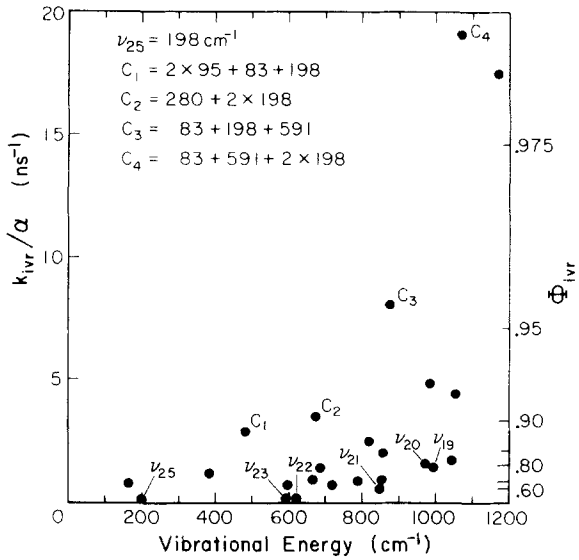

FIG. 8. Rate and quantum yield of IVR as a function of S_1 vibrational energy. The rate is expressed as a function of α which includes the radiative rate constants from the $|s\rangle$ and $\{|l\rangle\}$ states as well as any systematic errors involved in distinguishing between relaxed and unrelaxed fluorescence in SVL dispersed fluorescence spectra.

to also encompass any uncertainties involved in determining the other terms in Eq. (16). The value of α should be relatively constant with energy and in the ideal case is equal to unity.

The values of Φ_{IVR} and k_{IVR} below the barrier to isomerization, where unrelaxed fluorescence could still be detected, are tabulated in Table II (with error estimates) and plotted in Fig. 8. These data provide evidence for state-selective IVR. One finds that IVR is most extensive from S_1 levels involving combinations with low frequency vibrations. This is perhaps not surprising since the density of bath states is due primarily to low frequency vibrations. Consequently, initially excited low frequency combination states will have good Franck–Condon overlap with the bath states. In Fig. 9,

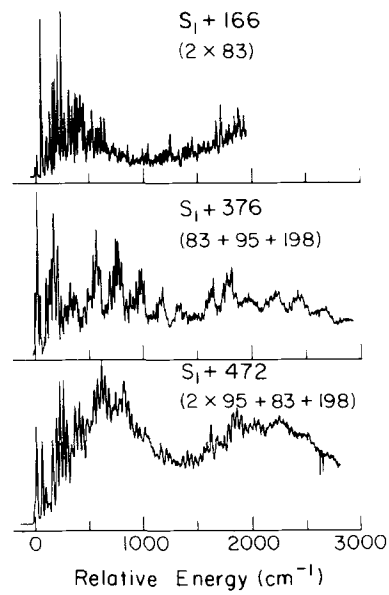

FIG. 9. Dispersed fluorescence spectra from vibronic levels consisting of combinations of low frequency modes. The spectra illustrate the appearance of relaxed fluorescence arising from efficient IVR from these optically active combination bands. Monochromator resolution was 0.5 Å.

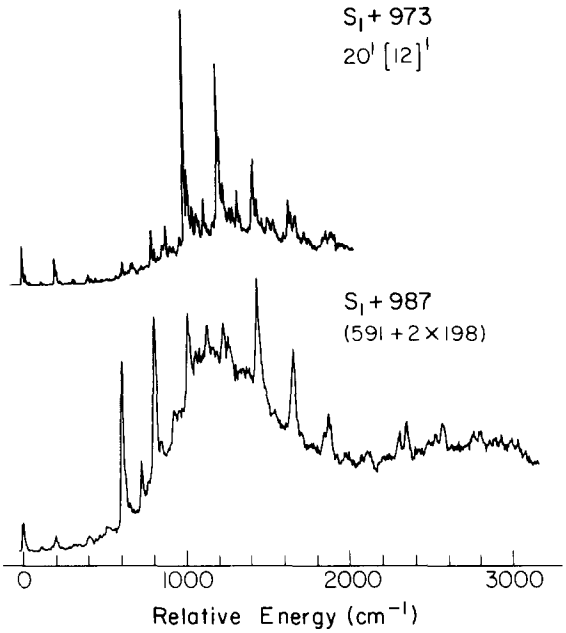

FIG. 10. Manifestation of state selective IVR. Dispersed fluorescence spectra at similar excess energies illustrates the greater yield of relaxed fluorescence, and hence IVR, from vibronic levels consisting of combinations compared to fundamentals. Monochromator resolution was 1.0 Å.

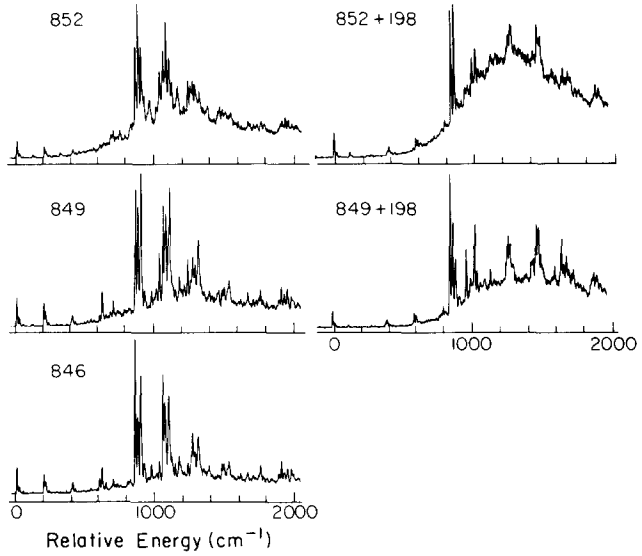

FIG. 11. Dispersed fluorescence spectra resulting from excitation of states that are coupled by Fermi resonance. Although the qualitative similarity of the spectra for $S_1 + 846$, 849, and 852 cm^{-1} attests to the Fermi resonance coupling, the difference in the relaxed fluorescence indicates that components that contribute to IVR exist in different amounts in the mixed states. The same behavior is observed for these states in combination with the 198 cm^{-1}, ν_{25}, fundamental. Monochromator resolution was 0.5 Å.

SVL dispersed fluorescence spectra are illustrated which show that IVR from low frequency combination states can be extensive even at low energies. Much of the apparent broadening in Fig. 9 may be due to spectral congestion, especially since the low frequency S_0 modes are very active in these spectra. However, qualitatively there is a clear trend toward increasing broad fluorescence with E_x. Since, our monochromator resolution and the low frequency intervals are similar at these higher energies, we conclude that the additional broadening is due mostly to relaxed fluorescence. (These conclusions are substantiated by more recent direct time-resolved data on jet-cooled *t*-stilbene.[14b]) Fundamental vibrations account for the lowest yields of IVR. This is illustrated in Fig. 10 where the fluorescence spectrum from a combination state shows substantially more broadening than that observed from a fundamental of nearly equal energy.

Another indication of state-selective IVR is displayed in Fig. 11 which contains SVL fluorescence spectra resulting from excitation into the Fermi resonance states at 846,849, and 852 cm^{-1}. (The nature and assignment of these levels are treated in the preceding paper.[1]) Although the unrelaxed (sharp) fluorescence structure is similar as a result of the strong Fermi resonance, a distinct difference is evident in the relaxed (broad) fluorescence. The same trend is observed when these states are excited in combination with the 198 cm^{-1} vibration (Fig. 11). Presumably, the Fermi resonance involves mixing of a fundamental with combination states. One might then assume that the major components of the 846 and 852 cm^{-1} mixed states are the fundamental and combination states, respectively.

In Fig. 8, an apparent onset to rapid IVR (< 100 ps) is indicated at about 1000 cm^{-1} including modes that may be fundamentals. Above the isomerization barrier ($E_x \geqslant 1200$ cm^{-1}), the dispersed fluorescence spectra are completely broad as evident in the examples presented in Fig. 12. We estimate that $k_{IVR} \approx 10^{11}$ s^{-1} (i.e., ~ 10 ps) at about 1400 cm^{-1}. Recent pump-probe picosecond experiments in this

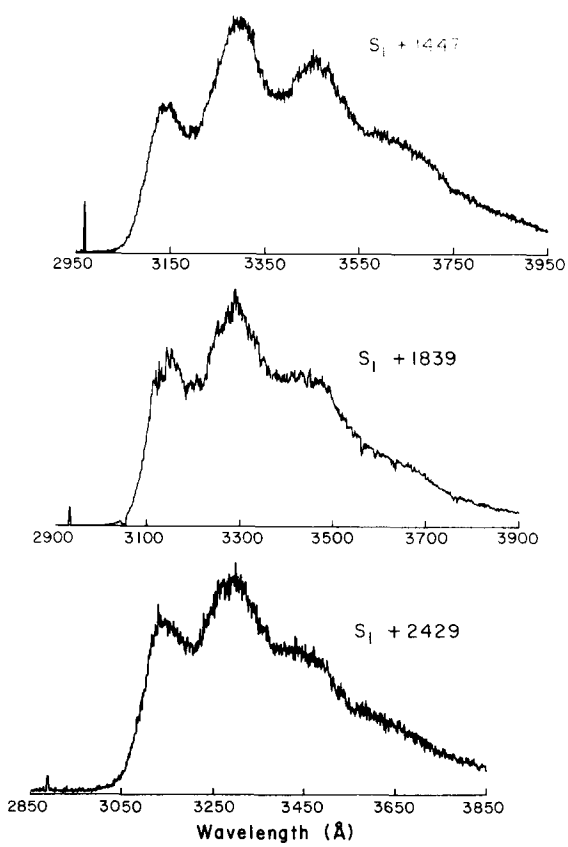

FIG. 12. Examples of dispersed fluorescence spectra at excitation energies above the threshold to isomerization. Note the absence of any detectable unrelaxed fluorescence. The sharp signal at the beginning of each spectrum is scattered laser light which was used to mark the excitation wavelength. No evidence of resonance fluorescence was observed at these energies.

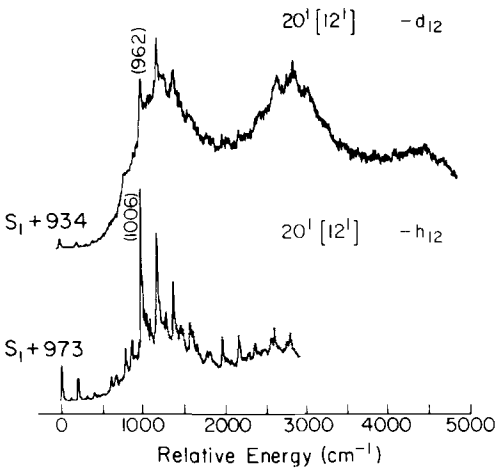

FIG. 13. Comparison of the dispersed fluorescence spectra of the $-h_{12}$ and $-d_{12}$ *t*-stilbene following excitation of the $\nu_{20}[\nu_{12}]$ fundamental. Although of similar S_1 vibrational energy, the $-d_{12}$ spectrum exhibits substantially more relaxed fluorescence than in $-h_{12}$. Monochromator resolution was 1.0 Å.

lab[14] have directly measured vibrational-rotational energy redistribution giving a characteristic time of ≈ 2 ps at $E_x \approx 2000\ \text{cm}^{-1}$.

Finally, we comment on the apparently greater yield of IVR that occurs in *t*-stilbene-d_{12} compared to the $-h_{12}$ compound. An example of this behavior is illustrated in Fig. 13. The vibrational frequencies in *t*-stilbene decrease upon deuteration and hence lead to an increase in the density of states. In Fig. 14, we have plotted the calculated density of states for *t*-stilbene-h_{12} and $-d_{12}$. At an excess energy of $\approx 950\ \text{cm}^{-1}$ (corresponding to the excitation energy of the $20^1[12^1]$ in h_{12} and d_{12} in Fig. 13), one obtains the ratio $\rho(h_{12})/\rho(d_{12}) \approx 3$. The ratio of $\Phi_{\text{IVR}}(h_{12})/\Phi_{\text{IVR}}(d_{12}) \approx 8$ derived from integrated fluorescence intensities is consistent with a density of states argument. The discrepancy is probably within experimental error, however, it is possible that the effective density of states is higher in the d_{12}.

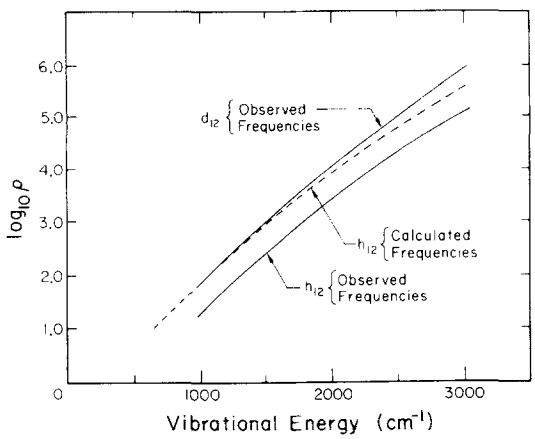

FIG. 14. Dependence of the density of states on vibrational energy for *t*-stilbene-h_{12} and $-d_{12}$. The computation of the densities of states was performed using a direct count (frequency grouped) procedure using all the vibrational frequencies of the molecule. Two sets of input frequencies were employed: calculated frequencies from Ref. 35; and observed frequencies from this and other work (see the text). By observed we mean substitution of the observed 83 and 95 cm^{-1} modes for the calculated 41 and 55 cm^{-1} modes (this, of course, will lower the calculated ρ values).

C. Dynamics and nature of the potential energy surface for isomerization

In the kinetic analysis that follows, we are concerned only with the energy region above the isomerization threshold (i.e., $E_x \geqslant 1200\ \text{cm}^{-1}$). In this region, IVR is rapid (Sec. IV B) on a reaction time scale, hence we may consider the initial reactant to be the manifold to redistributed states, $\{|l\rangle\}$. It is helpful to refer to Fig. 5 during subsequent discussions. An approximate potential energy surface along the reactive ethylene twist coordinate is presented in Fig. 1 to illustrate the crossing between the $B_u S_1$ state and a higher A_g state.

1. Rate parameters and RRKM calculations

a. Threshold energy: Barrier height for isomerization. Our measured energy dependent fluorescence decay rates are compiled in Table III and plotted in Fig. 4. The rate constant for fluorescence decay k_{fl} (Table III) for reactive energies (i.e., $\geqslant 1200\ \text{cm}^{-1}$) represents from the $\{|l\rangle\}$ states and hence k_{fl} is equivalent to the decay eigenvalue λ_l in our kinetic model [Eq. (11)]. The nonradiative rate constant k_{nr} in Table III is determined by subtracting from k_{fl} the 0^0 level fluorescence rate constant which we take to be the radiative rate constant k_{rad}. The absolute quantum yield for the 0^0 level has been determined to be unity by Amirav and Jortner.[17]

The abrupt increase in the nonradiative rate above $E_x \approx 1200\ \text{cm}^{-1}$ indicates a sharp threshold process which we attribute to isomerization. Other nonradiative processes appear to be negligible (or are at least energy independent) judging by the constant values of k_{fl} below the threshold energy. The values of k_{nr} reported in Table III may be associated with the expression $\lambda_l - k_{lg}$ in Eq. (11b). Various kinetic parameters which we shall be discussing below are summarized in Table IV. The threshold of 1100–1200 cm^{-1} (3.3 ± 0.2 kcal/mol) observed in this work and in our earlier report[2] represents the first direct measurement of the barrier height to the reaction in the isolated molecule.

The threshold energy of $E_0 = 3.3 \pm 0.2$ kcal/mol which we observe is in accord with solution phase activation energies which vary from 2.6 to 4.0 kcal/mol.[6–9,25] It is important to note that the differences in the activation energies observed in solution may be due to the nature of the barrier which results from a crossing of the B_u and the A_g electronic surfaces (Fig. 1). The energies of these two states have differ-

TABLE IV. Some properties of the excited state of isolated *t*-stilbene.

	h_{12}	d_{12}
λ_{00}	3101.4 Å	3092.5 Å
E_0[a]	3.3 ± 0.2 kcal/mol	
A_{lp}[a]	$1.6 \pm 0.4 \times 10^{11}\ \text{s}^{-1}$	
τ_{rad}[b]	2.67 ± 0.1 ns	2.53 ± 0.1 ns
K_{lp}[c]	>1	

[a] Solution phase values for E_0 and A_{lp} range from 2.6–4.0 kcal/mol and 1×10^{12}–$5 \times 10^{12}\ \text{s}^{-1}$ (Refs. 4–9).

[b] We take the 0^0 level fluorescence decay time to be the radiative time constant.

[c] Equilibrium constant $K_{lp} \equiv k_{lp}/k_{pl}$. The limit applies to energies above E_0.

ent solvent dependencies. Consequently, the energy of the crossing and therefore the barrier to isomerization may be solvent dependent. This behavior is particularly evident in the related molecule diphenylbutadiene, where the ordering of the B_u and the A_g energies are actually reversed in the vapor and solution phases.[15,31] Solution phase studies can also be problematic in the sense that an increase in temperature leads to a decrease in viscosity. This can give rise to reaction rates that are greater than expected on the basis of thermal activation alone, especially for stilbene where large amplitude torsional motions are strongly affected by solvent viscosity. Consequently, Arrhenius plots when uncorrected for viscosity may tend to overestimate the true barrier height.[32a]

Recently, Amirav and Jortner[17] found from relative quantum yield measurements, an onset to nonradiative decay in jet-cooled *t*-stilbene that is in agreement with our results. They cite a threshold of 900 cm^{-1} for isomerization based on a best fit RRK analysis of their data, although a sharp decrease in the quantum yields in their study was apparent at a value closer to 1200 cm^{-1}. Khundkar *et al.*,[33] have recently analyzed our earlier *t*-stilbene data[2] using an RRK analysis and likewise obtained a best fit for $E_0 = 900$ cm^{-1}. In another picosecond/jet study of a reactive molecule,[19] we found that the best fit RRK analysis yielded a threshold value smaller than indicated by the onset of nonradiative decay. As a further test of the accuracy of the RRK method for isolated molcules, we calculated RRKM rates of *t*-stilbene isomerization assuming a barrier of 1150 cm^{-1} and again found that the RRK analysis underestimated the true barrier.

We observe a slight onset for nonradiative decay at $E_x \approx 1100\ cm^{-1}$, however even at $E_x = 1170\ cm^{-1}$ the nonradiative rate is only $k_{nr} \approx 6\times 10^7\ s^{-1}$ (Table III). This value is on the order of the nonradiative rates measured in unreactive molecules at energies corresponding to a similar density of states [e.g., anthracene; $k_{nr} \approx 6\times 10^7\ s^{-1}$ ($E_x \approx 1200\ cm^{-1}$), $k_{nr} \approx 2\times 10^8\ s^{-1}$ ($E_x \approx 3000\ cm^{-1}$).][21] At $E_x = 1048$ cm^{-1}, we observe no measurable nonradiative decay relative to the 0^0 level. We, therefore, conclude that the slight increase in k_{nr} is probably due to unreactive processes whereas the sharp increase in k_{nr} at $E_x \approx 1100$–$1200\ cm^{-1}$ reflects the threshold to isomerization.

b. Simple rate equations. It has recently been shown[34] that an activation-type rate equation of the form

$$k(E_x) = Ae^{-nE_0/E_x} = Ae^{-E_0/kT_{eff}} \tag{17}$$

can be used to describe the excess energy E_x dependent rates in isolated isoenergetic molecules. In Eq. (17) an average temperature is defined according to the number of effective vibrations n. The terms E_0 and A are the energy threshold and preexponential frequency factor, respectively. The analysis of k_{nr} (Table III) by Eq. (17) is illustrated in Fig. 15 and leads to the values $A = 1.6\times 10^{11}\ s^{-1}$ and $n = 7.7$. It is important to note that we do not at this point equate k_{nr} (and therefore A) strictly to the forward rate constant for isomerization k_{lp}, since the role of reversibility [i.e., k_{pl}, Eq. (11b)] has not yet been addressed (cf. Sec. IV C 3).

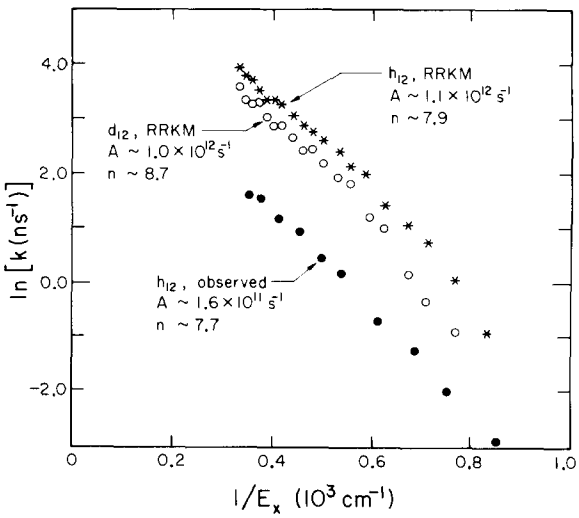

FIG. 15. Effective temperature analysis of reaction rates as a function of E_x. The data were analyzed according to Eq. (17) using a barrier of $E_0 = 1150$ cm^{-1}. The symbols used to denote the RRKM data correspond to the set of data plotted in Fig. 16.

Khundkar *et al.*[33] recently compared the time-resolved measurements of jet-cooled *t*-stilbene isomerization[2] to calculated rates using the RRKM expression

$$k(E_x) = \frac{N^{\#}(E^+)}{h\rho(E_x)}, \tag{18}$$

where $N^{\#}(E^+)$ is the total number of quantum states in the transition state in the energy region $E^+ = E_x - E_0$ (where E_0 is the barrier to reaction) and $\rho(E_x)$ is the density of states of the reactant at excess energy E_x. A direct count of the quantum states was employed in the earlier work[33] using the calculated frequencies of Warshel.[35] These authors found that the calculated rates were greater than the observed rates by nearly an order of magnitude.[33]

The low frequency vibrations which most strongly affect the outcome of the calculations have only recently been studied in detail in *t*-stilbene.[1] The RRKM rates were, therefore, recalculated by substituting the observed low frequency vibrations reported in the previous paper[1] for Warshel's calculated values. In the case of unobserved vibrations (particularly the nontotally symmetric modes), the observed ground state frequencies from Raman/IR work[36] were used. Some uncertainty still exists in assigning some of the observed frequencies to Warshel's calculations and hence different possibilities were considered in the RRKM calculations. A comparison of the various RRKM results with our observed decay rates for *t*-stilbene-h_{12} is given in Fig. 16 (also included are calculated rates for -d_{12}). In all cases, the revised calculations varied by no more than 20% from those calculated by Khundkar.[33] We also investigated the effect of anharmonicities on the sum and density of states quantities in Eq. (18). Using an average vibrational bond energy of 100 kcal/mol in the reactant and transition state, we obtained rates that were about 10% slower than those obtained assuming harmonic vibrations. The decrease in the calculated decay rates for *t*-stilbene-d_{12} compared to -h_{12} is a result of the decrease in the frequency of the reactive C_e–C_e torsion

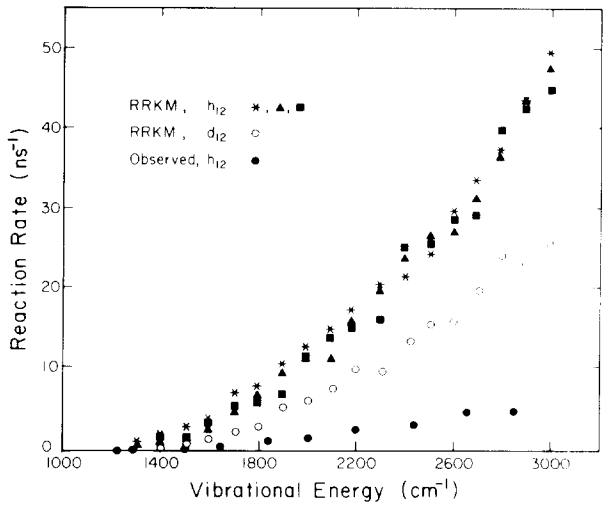

FIG. 16. Comparison of observed and calculated (RRKM) reaction rates as a function of excess energy. Three models for the input frequencies of *t*-stilbene were employed: (▲) calculated frequencies from Ref. 35; (*) observed frequencies where the 83 and 95 cm^{-1} modes are assigned to the calculated 41 and 55 cm^{-1} frequencies; and (■) observed frequencies where the 39, 83, and 95 cm^{-1} modes are assigned to the calculated 41, 55, and 88 cm^{-1} frequencies. The *t*-stilbene-d_{12} calculations (○) are the analog of the (*)-h_{12} calculations. The lack of smoothness of the RRKM data is the result of the routine for counting states which groups together fundamentals of similar frequencies.

modes[35] and the increase in the overall density of states (Fig. 9) due to deuteration.

It is evident in Fig. 16 that an order of magnitude discrepancy exists between the observed and RRKM rates for *t*-stilbene-h_{12}. When the calculated RRKM data are fit to Eq. (17) (see Fig. 15), the following values were obtained: $A_{lp}^{\text{calc}} = 1.1\times10^{12}\ s^{-1}$ and $n^{\text{calc}} = 7.9$ for -h_{12} and $A_{lp}^{\text{calc}} = 1.0\times10^{12}\ s^{-1}$ and $n^{\text{calc}} = 8.7$ for -d_{12}. Note that the calculated results refer to the forward rate constants for isomerization k_{lp} (cf. Fig. 5). In accord with the earlier RRKM[33] study, the frequency factor A for the RRKM data is about an order of magnitude greater than that for the observed data. A_{lp}^{calc}, however, is in very good agreement with observed solution phase results, which except for one study,[6] place this value between 1×10^{12} and $5\times10^{12}\ s^{-1}$.[7-9] We address this situation in the following sections.

2. Effect of the solvent

Our time-resolved jet results have been compared with solution phase studies above in regard to the reaction barrier E_0 and the frequency factor A. It is of interest, however, to compare specific reaction rates by relating temperature in the solution (or vapor phase bulb experiments) to an average vibrational energy E_V which can in turn be associated with specific vibrational energy in the jet-cooled molecules. In a statistical thermodynamic model, the vibrational contribution to the total energy of a molecule is given by

$$E_V = Nk\sum_i \frac{\Theta_i}{e^{\Theta_i/T}-1}, \tag{19}$$

where $\Theta_i = h\nu_i/k$. This procedure has been used recently to relate our earlier jet results[2] to a pump-probe ionization experiment in a bulb.[14a] Here, we extend the method to include temperature dependent rate measurements of *t*-stilbene in solution. A compilation of time-resolved data in the jet, vapor phase bulbs and solution are illustrated in Fig. 17.

The average vibrational energy in a thermal sample actually encompasses a wide distribution of energies, whereas the fixed energies in the jet may be thought of as an average energy with a very narrow distribution. Consequently, a direct comparison in terms of average vibrational energies (irrespective of distribution) is not rigorously correct. We therefore consider two models. First is the calculated dependence of the thermal rate constant $k(T)$ on the average vibrational energy for a room temperature collisionless bulb experiment in Fig. 17 (solid line) as outlined elsewhere.[14a] Second are the thermally averaged RRKM rate constants $k_{\text{RRKM}}(T)$ (dashed line) which we use to compare with the solution phase data. These were obtained by averaging the calculated energy dependent rate constants $k_{\text{RRKM}}(E_x)$ over a Boltzmann distribution according to the expression

$$k(T) = \frac{1}{Q}\int_0^\infty k(E_x)\rho(E_x)e^{-E_x/kT}\,dE_x. \tag{20}$$

It is apparent in Fig. 17 that the rates in solution are substantially faster than in the vapor phase (either in the jet or the bulb). This is different from results which indicate[19,37] that the solvent should impede the reaction rate (particularly when large amplitude torsional motions are involved) simply due to viscosity. A viscosity dependence for *t*-stilbene is clearly indicated from the data of Rothenberger *et al.*[38]

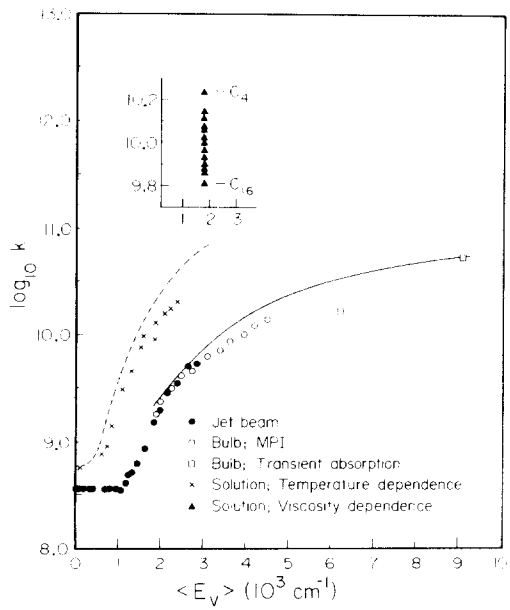

FIG. 17. Comparison of time-resolved data for *t*-stilbene isomerization in a jet, in a vapor phase bulb, and in solution. Jet results, this work (●); bulb results, Ref. 14(a) (○), Ref. 16 (□); solution results (in 3:2 methylcyclohexane/isohexane), Refs. 7 and 8 (×). Viscosity dependent rate data derived from Ref. 38 (▲) are plotted in the insert for a series of C_n-alkane solvents. The calculated curves repesent:(—) the average of the energy specific rate constants $k(E_x)$ to a thermal distribution $k(T)$ at room temperature [see Ref. 14(a)]; and (---) best curve through the thermalized RRKM calculated rate constants [Eq. (20)]. The latter curve includes the solution phase radiative rate of 0.6 ns^{-1}.

which we have plotted in the insert in Fig. 17. Finally, we mention that the thermally averaged RRKM results are in good agreement with the solution phase results. A discussion of why the reaction rates are impeded in the vapor phase is presented in the following.

D. The adiabaticity of the surface crossing

There are a number of properties of the isolated molecule that can account for different rate behavior compared to solution phase. The important questions which must be addressed are:

(i) Is the surface crossing involving B_u and A_g avoided (i.e., adiabatic, solid line in Fig. 1) or allowed (i.e., diabatic, dotted line)? Is it reasonable to expect that the solvent can alter the adiabaticity of the reaction?

(ii) Is the reaction to an excited state perpendicular geometry (i.e., $\{|p\rangle\}$) reversible in isolated *t*-stilbene? In the isoenergetic molecule, the ratio of the forward to reverse rate constants (defined loosely as an "equilibrium constant" in the isolated molecule) is governed by the relative density of states in the two manifolds, which is an *entropy* effect (though indirectly related to enthalpy).

(iii) What is the lifetime of the $\{|p\rangle\}$ states in the isolated molecule? This can have profound effects on the relation between the observed rates and the actual rate of forward reaction k_{lp} [Eq. (11b)] if reversibility exists. We address these questions as they relate to isolated vs solution phase *t*-stilbene next.

Frequent reference to Figs. 1 and 5 will be made throughout this section. It is worthwhile at this point to sort out the meaning of the various decay parameters defined in Sec. IV A. The terms Λ_l and Λ_p represent the total rate constant for decay from $\{|l\rangle\}$ and $\{|p\rangle\}$, respectively [Eqs. (6c) and (6d)]. The observed decay constants λ_l and λ_p approximately equal Λ_l and Λ_p when $K_{lp} = k_{lp}/k_{pl} \gg 1$ (i.e., reversibility is slight) and become equivalent in the limit where $K_{lp} \to \infty$ [cf. Eq. (6e)]. In cases where $K \ll 1$, Λ and λ generally bear no simple relation. A variety of situations are illustrated in Figs. 6 and 7. As a result of these considerations, the observed fluorescence decay constants k_{fl} which we associate with λ_l [$k_{nr} \equiv \lambda_l - k_{lg}$, Eq. (11b)] may not necessarily be an accurate measure of the forward rate constants for isomerization k_{lp}. Our intent in the following is to determine the energy dependence of k_{lp} and relate this information to the questions posed above.

1. Reversibility

Solution phase studies on *t*-stilbene isomerization are strongly divided on the question of reversibility. Much of the disagreement has arisen from early work which indicated that the fluorescence decays were biexponential.[6,7] By assuming that the decay from the twisted or perpendicular ($\vartheta = 90°$) states $\{|p\rangle\}$ is not very fast (i.e., $k_{pg} \approx k_{lp}$), the biexponential decays were interpreted to be due to back reaction k_{pl}. We have calculated the time dependence of the reactant $\{|l\rangle\}$ and perpendicular $\{|p\rangle\}$ states as a function of the reverse rate constant k_{pl} which we illustrate in Fig. 6. When decay from $\{|p\rangle\}$ is slow, a noticeable biexponential decay is predicted which depends on the extent of the reverse reaction.

More recent work has established that the true fluorescence decay in solution is single exponential,[8] thus concluding that reversibility is negligible. This criterion alone, however, is not sufficient to judge reversibility to be minor. For example, if the rate of decay from $\{|p\rangle\}$ is much greater than from $\{|l\rangle\}$ (i.e., $\Lambda_p \gg \Lambda_l$), then single-exponential decay from $\{|l\rangle\}$ will be observed regardless of the value of k_{pl}. The calculated curves in Fig. 7 illustrate this situation (a slight biexponential component of relative magnitude Λ_l/Λ_p is evident at very early time). A single exponential decay constant λ_l may be observed which clearly varies with k_{pl} [also indicated by Eq. (11b)]. Recent evidence indeed indicates that $\{|p\rangle\}$ decays rapidly (< 20 ps) by internal conversion to the ground electronic state.[39] Hence, the extent of reversibility in solution is still not well established. Perhaps the strongest evidence in favor of minor reversibility in solution is the close agreement of the solution phase decay rates with the RRKM rates calculated for the forward rate constant k_{lp} (Sec. IV C 1).

Reversibility is difficult to assess in the isolated molecule. Unlike in solution, reactions in isolated molecules are isoenergetic and therefore the effect of enthalpy takes the form of entropy in that the density of states ρ in the $\{|l\rangle\}$ and $\{|p\rangle\}$ manifolds at a given energy will be different. If we assume for simplificity that the vibrational frequencies are the same in both manifolds, then the entropy contribution to isomerization due to ρ may be expressed as

$$\Delta S_\rho = -R \ln \frac{\rho(E_x + \Delta E_0)}{\rho(E_x)}, \tag{21}$$

where ΔE_0 is the difference in the threshold energies for the forward and reverse pathways and may be likened to the enthalpy of the process. The equilibrium constant will also be influenced by entropy effects such as geometry, which we designate as ΔS_{geo}. In solution, due to vibrational relaxation, ΔS_ρ is minimal and therefore the entropy is dominated by ΔS_{geo}. In isolated, isoenergetic molecules, the equilibrium constant is given by

$$K = \exp(\Delta S_\rho + \Delta S_{geo})/R. \tag{22}$$

The computed density of states, used earlier in the RRKM calculations and illustrated in Fig. 14, increase approximately exponentially in the low energy region and for *t*-stilbene-h_{12} fit reasonably well (within the accuracy of the computation) to the expression

$$\ln \rho(E_x) = 0.0042\, E_x. \tag{23a}$$

This leads to the relation

$$\Delta S_\rho = -0.0042 R \Delta E_0. \tag{23b}$$

Equation (23b) is only approximate since ΔS_ρ is expected to have a slight dependence on E_x however, the relation is sufficient for our needs. The remaining information required to calculate K_{pl} are the thermodynamic quantities for enthalpy and S_{geo}. Unfortunately, for *t*-stilbene these values are not well defined. The two sets of data reported in the literature ($\Delta H = +1.75$ kcal/mol, $\Delta S = +10.6$ e.u.)[25] and ($\Delta H = -3.3$ kcal/mol, $\Delta S = -2.0$ e.u.)[6] differ consider-

ably. The former study has been criticized in the literature.[6–8,26] The entropy change also appears to be unreasonably large. We therefore favor the latter data from which we obtain the result $K_{lp}^{calc} \approx 50$. Using the former set of data also gives a forward equilibrium constant of ≈ 15. Hence, based on our model for the density of states and the thermodynamic values reported from other work,[6,25] we conclude that reversibility is not a significant factor in our kinetic model. Consequently, we may view the observed nonradiative rates (Table III) as being due predominately to the forward rate constant k_{lp} [Eq. (11b)].

2. Lifetime of $\{|p\rangle\}$

Both the lifetime of $\{|p\rangle\}$ and the magnitude of the reverse rate constant k_{pl} come into play in determining the extent to which biexponential behavior might be observed (Figs. 6 and 7). In previous studies, there has been considerable uncertainty regarding the rate of internal conversion of $\{|p\rangle\}$ to the ground state; some kinetic analyses indicating slow rates ($k_{pg} \approx 10^8$–10^9 s^{-1}).[6,7a,8b,25]

Recent time-resolved studies[39] strongly indicate, at least in solution, that the lifetime of $\{|p\rangle\}$ is very short (<20 ps) due to internal conversion to a maximum in the ground electronic surface (Fig. 1) where it then branches to form both *cis* and *trans* isomers (in nearly equal proportion[5]). In the isolated molecule, the $\{|p\rangle\}$ states may be longer lived. It is difficult to estimate the lifetime of $\{|p\rangle\}$ in our study since we do not directly probe these states. The observation of single exponential fluorescence decays indicates that either reversibility k_{pl} is negligible [Fig. 6(a), $x=0$ curve] *or* that decay of $\{|p\rangle\}$ A_p is very rapid [Fig. 7(a)]. Since, we have concluded that reversibility is minor, it is not possible to determine with accuracy the lifetime of $\{|p\rangle\}$.

There are a number of reasons, however, to expect that the lifetime of $\{|p\rangle\}$ is short:

(i) the excited state minima at $\vartheta = 90°$ represents an avoided crossing with the ground state maxima. If we were to imagine the doubly excited A_g state for *trans* or *cis* geometry to involve two antibonding orbitals, then a 180° twist would correlate with two bonding orbitals corresponding to the *cis* and *trans* ground states. Calculations have shown using this model that the lifetime of the perpendicular excited state is on the order of 1 ps.[40]

(ii) As a result of the relatively small energy gap due to the avoided crossing between the excited and ground A_g states, the rate of internal conversion should be much faster at $\vartheta = 90°$ then at any other point along the reactive potential surface.

(iii) Vibronic interactions are increased for twisted geometries as a result of reduced symmetry. Other evidence suggesting that $\{|p\rangle\}$ is short lived in the vapor consists of a lack of observations of transient absorption[16] or ionization[14] signals (so far) corresponding to this species.

3. Deviations from RRKM behavior

a. Diabaticity: Landau–Zener–Stueckelberg treatment. The different rates of reaction that are observed in the vapor and solution phase may be explained by examining characteristics of the surface crossing in these two phases. An excellent recent treatment of the surface crossing problem is given in another context by Frauenfelder and Wolynes.[41] We begin by assuming that in the absence of an interaction V_{12} between the excited B_u and A_g states, that the nature of the crossing is allowed (diabatic). If $V_{12} \neq 0$, the curves will repel to give a splitting of $\Delta = 2|V_{12}|$ at the crossing (Fig. 1).

On the basis of symmetry alone, the excited B_u, A_g surface crossing is allowed for a planar (C_{2h}) molecular geometry as well as for geometries in which the phenyl groups are rotated out-of-plane (C_2 or C_i, depending on the phase of rotation) since the two electronic states still correlate with different irreducible groups. In these cases, the system might be expected to proceed to the upper surface in passing through the crossing (nonadiabatic transition). If the two surfaces are strongly repulsive at the crossing either through a large interaction or a highly distorted geometry which breaks the symmetry allowedness, the molecule will stay on the lower surface in traversing the crossing region (adiabatic transition). The degree of adiabaticity expected for intermediate cases depends on the dynamics of the trajectories through the crossing region.

One may define an adiabaticity factor γ based on the uncertainty principle.[41] If a system spends a time in the mixing region that is long compared to the inverse of the splitting (i.e., $\gamma = \Delta\tau \gg 1$) then the transition will be adiabatic. Physically, this is because the system has sufficient time to find the path of minimum energy. The time τ depends on the velocity v through the crossing region and the interaction length l since $\tau = l/v$. The interaction length will increase with Δ but decrease with the difference in slopes of the two surfaces at the crossing $|F_2 - F_1|$ and is therefore defined[41] by

$$l = \frac{\Delta}{|F_2 - F_1|}. \tag{24}$$

Consequently the *adiabaticity* factor may be expressed as

$$\gamma = \frac{\Delta\tau}{\hbar} = \frac{\Delta^2}{\hbar v |F_2 - F_1|}. \tag{25}$$

This provides a satisfactory criteria for adiabatic ($\gamma > 1$) and nonadiabatic ($\gamma < 1$) transitions. The same considerations are embodied in the Landau–Zener–Stueckelberg (LZS) expression for *nonadiabatic* transition probabilities[42,43] given by

$$P_{12} = \exp\{-\pi \tfrac{1}{2}\gamma\}. \tag{26}$$

This expression is valid only when P_{12} is nearly unity ($\gamma \ll 1$).

We now examine the possibility that the isomerization of *t*-stilbene is nonadiabatic in the isolated molecule and is made adiabatic in solution due to different dynamics of the trajectory through the crossing, namely due to the velocity. The velocity v in the isolated molecule is dependent upon the frequency of the reactive vibration and the distribution of energy among the other modes of the molecule.[44] Accurate determinations of v are difficult and require sophisticated models for energy redistribution, however, a reasonable estimate may be obtained by assuming a statistical distribution and assuming that the fraction of energy in the reactive mode is proportional to the ratio of the density of states containing

the reactive coordinate to the total density of states. This ratio is calculated to be approximately 1/10 in the energy region of $1500 \leqslant E_x \leqslant 2500\ \mathrm{cm}^{-1}$ and is consistent with there being about ten effective oscillators over this energy region. Other evidence supporting this result are: (i) the calculated average vibrational energy for *t*-stilbene at room temperature (see Fig. 17) is $\approx 1900\ \mathrm{cm}^{-1}$ (i.e., $\approx 10kT$); and (ii) an effective temperature analysis of the observed isomerization rates gives a value of $n \approx 8$ (cf. Fig. 15 and Sec. IV C 1 *b*).

The experimental non-RRKM rates of isomerization in the isolated molecule, which are an order of magnitude slower than solution rates, and RRKM calculations (see Fig. 17) may be represented by a nonadiabatic transition probability of $P_{12} \approx 0.9$ in the LZS model of Eq. (26). Given values for the other parameters in this expression, we may estimate the energy gap Δ at the crossing which is consistent with this P_{12} value. At a particular energy, say $E_x = 2000\ \mathrm{cm}^{-1}$, the energy in the reactive coordinate will be about $200\ \mathrm{cm}^{-1}$. In terms of an angular velocity, this is estimated to be on the order of $v \approx 4 \times 10^{13}$ rad/s.[45] A value of $|F_2 - F_1| \approx 15\,000\ \mathrm{cm}^{-1}/\mathrm{rad}$ is obtained from Fig. 1, which represents our best estimate of the reactive surface based on available information.[11,12,40]

Using the above results, these data are consistent with an energy gap of Δ of roughly $1000\ \mathrm{cm}^{-1}$. That this is a reasonable value suggests that a diabatic representation for isomerization in the vapor phase is plausible. In solution, the effective velocity v_{eff} may be much less than v due to solvent viscosity (high friction limit). Consequently, the solvent friction can change a nonadiabatic transition into an adiabatic one, thus explaining the much faster isomerization rates in solution. For instance the validity of the LZS model [Eq. (26)] breaks down for reasonable solution phase velocities of $v_{\mathrm{eff}} \leqslant 0.1v$. Furthermore, the solvent interaction can *relax* the diabatic crossing in other ways. For example, since the twisting of the molecule in solution is dependent on the interaction with the solvent.[32,38,46] a more distorted geometry (i.e., effective symmetry lowering) can occur thus creating a more avoided crossing and hence more adiabaticity. Finally, collision induced vibrational relaxation by the solvent can enhance the adiabaticity. In a very recent work by Majors *et al.*,[47] the energy dependent rates of *p*-methylstilbene were observed to be similar to those of stilbene, thus implying that the rates are not determined by the *total* density of states in the molecule (which increases with methyl substitution). These authors considered that the excited state B_u–A_g internal conversion may be responsible for this behavior. This is consistent with the above discussion on diabaticity.

b. IVR and other considerations. Earlier, we examined the possibility that the slow rate of isomerization in collisionless *t*-stilbene might be due to a high degree of reversibility of the reaction. The issue of reversibility is therefore an important one. We concluded that the equilibrium constant for isomerization was $K_{lp} \gg 1$ based on a density of states argument and reported enthalpies [Eqs. (21)–(23)]. The same qualitative conclusion can be reached simply on the basis of the fact that the excited state minimum represents an avoided crossing with the ground state surface and therefore should have an energy lower than the 0^0 level of the *trans* configuration (Fig. 1). The density of states at $\vartheta = 90°$ must therefore be greater than at $\vartheta = 0°$ thus supporting a forward equilibrium.

To explain a large discrepancy between observed and RRKM rates one must also look to nonstatistical IVR effects. Berne and DeLeon have shown that even if chaotic behavior occurs in a molecule, it may be restricted to only a part of the total phase space.[48] Such a system will react exponentially, but not be statistical in the sense that the decay rates for this situation will be *larger* than for RRKM theory. In other words, ρ in Eq. (18), will be smaller or "restricted" and hence the RRKM rates will increase. Hase[49] has discussed conditions in which nonstatistical behavior might lead to observed rates that are smaller than RRKM rates. In this case, however, the energy redistribution exhibits quasiperiodic behavior which gives rise to nonexponential decay. This situation may characterize certain molecules in the low friction limit. Although, we cannot rule out this possibility completely, it is arguable that these effects are *not* present in *t*-stilbene isomerization on the basis that: (i) only single exponential decays are observed on our time scale; (ii) quantum beats are absent above the reaction barrier; and (iii) dispersed fluorescence spectra and direct measurements[14] indicate that IVR is rapid and extensive at energies above the barrier.

V. SUMMARY AND CONCLUSION

The state-selective dynamics of *t*-stilbene photoisomerization were investigated using single vibronic level picosecond excitation in a supersonic jet. The experiments consisted of time-resolved measurements of the reaction rate as a function of vibrational energy, fluorescence quantum yield ratios from relaxed and unrelaxed vibronic levels, and an extensive vibrational analysis of excitation and dispersed fluorescence spectra (see the previous paper). The major conclusions drawn from this study are summarized as follows:

(i) The yield of IVR Φ_{IVR} appears to be state selective. The values of Φ_{IVR} for vibronic levels involving combinations of low frequency vibrations were much greater than that found for fundamental vibrational levels of similar energy. This behavior is attributed to good Franck–Condon overlap between combination bands involving low frequency modes and the bath states, since the density of bath states is dominated by low frquency modes. The observation of quantum beats in the fluorescence decay spectra of fundamentals is also indicative of restricted IVR at moderate excess energy (i.e., below the reaction barrier).

(ii) The IVR yield is significant at energies in excess of $\approx 1000\ \mathrm{cm}^{-1}$ and the rate is much faster than the reaction rate at all energies studied. This was apparent by comparing the IVR rates derived from the integrated fluorescence intensity of relaxed and unrelaxed emission to the direct time-resolved reaction rates. This result is also consistent with the absence of mode selective rates of reaction.

(iii) A sharp threshold for nonradiative decay, marking the onset of isomerization, was observed at 3.3 ± 0.2 kcal/mol (1100–$1200\ \mathrm{cm}^{-1}$). The radiative lifetimes measured from the 0^0 level fluorescence decays were 2.7 ± 0.1 ns (h_{12}) and 2.5 ± 0.1 ns (d_{12}). An analysis of the measured rates

using an effective temperature model led to a frequency factor of $A = 1.6 \pm 0.4 \times 10^{11}$ s^{-1} for *t*-stilbene-h_{12}. Using RRKM theory, these values were calculated to be $A = 1.1 \times 10^{12}$ s^{-1} (h_{12}) and 1.0×10^{12} s^{-1} (d_{12}).

(iv) The measured rates of isomerization in isolated *t*-stilbene are nearly an order of magnitude lower than those calculated (RRKM) or observed in solution.[7,8,26] A kinetic model based on a reactive surface which considers the crossing of excited B_u and A_g electronic states was adopted to examine the importance of reversibility of isomerization and the question of adiabaticity across the reaction barrier. Using a density of states and entropy argument it was determined that the "equilibrium" constant for isomerization is $K \gg 1$ indicating that reversibility is negligible.

(v) The ratio of ≈ 0.1 for the vapor to solution phase isomerization rate is interpreted in a diabatic (allowed crossing) representation and attributed to the adiabaticity (Landau–Zener) factor for traversing to the lower perpendicular surface (i.e., the nonadiabatic transition probability is 0.9). This value is consistent with an energy gap at the surface crossing of ≈ 1000 cm^{-1} if we adopt the qualitative surface in Fig. 1. The faster (adiabatic) rates in solution can be explained by a reduction in the velocity through the crossing region due to solvent viscosity. Other possibilities, such as reversible reaction and restricted IVR were also considered.

(vi) Comparison of the collisionless isomerization dynamics of styrene,[13] *t*-stilbene, and diphenylbutadiene[15] indicates that the relative energy of the B_u and A_g states, and therefore the barrier height due to the crossing, decreases with increasing conjugation.

The mechanism for isomerization may then be summarized as follows:

(i) Initially excited optically active $|s\rangle$ modes redistribute energy in the isolated molecule on the picosecond time scale. Fluorescence from optically active and equilibrated states $\{|l\rangle\}$ is evident and, therefore, we can rule out that $|s\rangle$ proceeds directly to product.

(ii) The equilibrated $\{|l\rangle\}$ states, which result from IVR undergo a twisting to an excited nonfluorescent perpendicular state derived from an A_g electronic state.

(iii) Collisionless isomerization proceeds at a much slower rate than in solution. This is attributed to a diabatic (allowed) surface crossing involving the initially excited *trans* B_u state and the perpendicular A_g state. In the isolated molecule, the diabatic reactive surface impedes the rate of isomerization, whereas in solution through collisions, the adiabaticity is recovered.

ACKNOWLEDGMENTS

We wish to acknowledge the support of this work by the National Science Foundation under Grant No. CHE-8211356. We are also grateful to Professor A. Warshel for illuminating discussions about nonadiabatic transitions and spectroscopy, Professor R. M. Hochstrasser for his interest in this work, and to Professor J. Jortner for providing us with a preprint of his paper. Finally, we wish to thank Professor P. G. Wolynes and Professor R. A. Marcus for enlightening discussions.

[1] J. A. Syage, P. M. Felker, and A. H. Zewail, J. Chem. Phys. **81**, 4685 (1984).
[2] J. A. Syage, Wm. R. Lambert, P. M. Felker, A. H. Zewail, and R. M. Hochstrasser, Chem. Phys. Lett. **88**, 268 (1982).
[3] G. Orlandi and W. Siebrand, Chem. Phys. Lett. **30**, 352 (1973).
[4] R. H. Dyke and D. S. McClure, J. Chem. Phys. **36**, 2326 (1962).
[5] J. Saltiel, J. D'Agostino, E. D. Megarity, L. Metts, K. R. Neuberger, M. Wrighton, and O. C. Zafiriou, Org. Photochem. **3**, 1 (1973); see also J. Saltiel and J. Charlton, in *Organic Chemistry* (Academic, New York, 1980) Vol. 42–3, p. 25.
[6] J. L. Charlton and J. Saltiel, J. Phys. Chem. **81**, 1940 (1977).
[7] (a) O. Teschke, E. P. Ippen, and G. R. Holtom, Chem. Phys. Lett. **52**, 233 (1977); (b) J. R. Taylor, M. C. Adams, and W. Sibbett, App. Phys. Lett. **35**, 590 (1979).
[8] (a) M. Sumitani, N. Nakashima, Y. Yoshihara, and S. Nagakura, Chem. Phys. Lett. **51**, 183 (1977); (b) F. Heisel, J. A. Miehe, and B. Sipp, *ibid.* **61**, 115 (1979).
[9] H. P. Good, U. P. Wild, E. H. Fisher, E. P. Resewitz, and E. Lippert, Ber. Bunsenges. Phys. Chem. **86**, 126 (1982).
[10] (a) G. Orlandi, P. Palmiari, and G. Poggi, J. Am. Chem. Soc. **101**, 3492 (1979); (b) F. Momicchioli, M. C. Bruni, I. Baraldi, and G. R. Corradini, J. Chem. Soc. Faraday Trans. 2, **70**, 1325 (1974); (c) G. Olbrich, Ber. Bunsenges. Phys. Chem. **86**, 209 (1982); (d) P. Tavan and K. Schulten, Chem. Phys. Lett. **56**, 200 (1978); (e) D. L. Beveridge and H. H. Jaffé, J. Amer. Chem. Soc. **87**, 5340 (1965).
[11] G. Hohlneicher and B. Dick, J. Photochem. (submitted).
[12] T. M. Stachelek, T. A. Pazoha, W. M. McClain, and R. P. Drucker, J. Chem. Phys. **66**, 4540 (1977).
[13] J. A. Syage, F. Al Adel, and A. H. Zewail, Chem. Phys. Lett. **103**, 15 (1983).
[14] (a) J. W. Perry, N. F. Scherer, and A. H. Zewail, Chem. Phys. Lett. **103**, 1 (1983); (b) N. F. Scherer, J. F. Shepanski, and A. H. Zewail, J. Chem. Phys. **81**, 2181 (1984).
[15] J. F. Shepanski, B. W. Keelan, and A. H. Zewail, Chem. Phys. Lett. **103**, 9 (1983).
[16] (a) B. I. Greene, R. M. Hochstrasser, and R. B. Weisman, J. Chem. Phys. **71**, 544 (1979); (b) Chem. Phys. **48**, 289 (1980).
[17] A. Amirav and J. Jortner, Chem. Phys. Lett. **95**, 295 (1983), and results to be submitted.
[18] T. S. Zwier, E. Carrasquillo M., and D. H. Levy, J. Chem. Phys. **78**, 5493 (1983).
[19] J. A. Syage, P. M. Felker, and A. H. Zewail, J. Chem. Phys. **81**, 2233 (1984).
[20] B. W. Keelan, J. A. Syage, J. F. Shepanski, and A. H. Zewail, *International Conference on Lasers* '83 (in press).
[21] W. R. Lambert, P. M. Felker, and A. H. Zewail, J. Chem. Phys. **81**, 2209, 2217 (1984).
[22] W. R. Lambert, P. M. Felker, and A. H. Zewail, J. Chem. Phys. **75**, 5958 (1981).
[23] (a) P. M. Felker and A. H. Zewail, Chem. Phys. Lett. **102**, 113 (1983); (b) **108**, 303 (1984); (c) Phys. Rev. Lett. **53**, 501 (1984).
[24] P. M. Felker, Wm. Lambert, and A. H. Zewail, J. Chem. Phys. (submitted).
[25] D. J. S. Birch and J. B. Birks, Chem. Phys. Lett **38**, 432 (1976).
[26] R. M. Hochstrasser, Pure Appl. Chem. **52**, 2683 (1980).
[27] T. Shibuya, Chem. Phys. Lett. **103**, 46 (1983).
[28] F. Lahmani, A. Tramer, and C. Tric, J. Chem. Phys. **60**, 4431 (1974); and references therein.
[29] We make use of the expansion for $x \ll 1$ that $(1 + 2x)^{1/2} \approx (1 + 2x + x^2)^{1/2} = (1 + x)$.
[30] K. F. Freed, Top. Appl. Phys. **15**, 23 (1976) and references therein.
[31] S. P. Velsko and G. R. Fleming, J. Chem. Phys. **76**, 3553 (1982); see also Ref. 37.
[32] (a) B. M. Ladanyi and G. T. Evans, J. Chem. Phys. **79**, 944 (1983); (b) D. C. Knauss and G. T. Evans, *ibid.* **74**, 4627 (1981).
[33] L. R. Khundkar, R. A. Marcus, and A. H. Zewail, J. Phys. Chem. **87**, 2473 (1983).
[34] (a) A. H. Zewail, Faraday Discuss. Chem. Soc. **75**, 315 (1983); (b) Laser Chem. **2**, 55 (1983).
[35] A. Warshel, J. Chem. Phys. **62**, 214 (1975).
[36] Z. Meić and H. Güsten, Spectrochim. Acta. Part A **34**, 101 (1978).
[37] S. H. Courtney, G. R. Fleming, L. R. Khundkar, and A. H. Zewail, J. Chem. Phys. **80**, 4559 (1984).
[38] G. Rothenberger, D. K. Negus, and R. M. Hochstrasser, J. Chem. Phys. **79**, 5360 (1983).

[39](a) M. Sumitani, N. Nakashima, and K. Yoshihara, Chem. Phys. Lett. **68**, 255 (1979); (b) M. Sumitani and K. Yoshihara, Bull. Chem. Soc. Jpn. **55**, 85 (1982).
[40](a) R. M. Weiss and A. Warshel, J. Am. Chem. Soc. **101**, 6131 (1979); (b) V. Bonaič-Koutecký, J. Köhler, and J. Michl, Chem. Phys. Lett. **104**, 440 (1984).
[41]H. Frauenfelder and P. G. Wolynes (preprint).
[42](a) W. G. Dauben, L. Salem, and N. J. Turro, Accs. Chem. Res. **8**, 41 (1975); (b) L. Salem, C. Leforestier, G. Segal, and R. Wetmore, J. Am. Chem. Soc. **97**, 479 (1975).
[43](a) J. C. Tully, in *Dynamics of Molecular Collisions, Part B*, edited by W. H. Miller (Plenum, New York, 1976), Chap. 4; (b) A. Warshel and M. Karplus, Chem. Phys. Lett. **32**, 11 (1975).
[44](a) R. A. Marcus, J. Chem. Phys. **62**, 1372 (1975); (b) S. A. Safron, N. D. Weinstein, D. R. Herschbach, and J. C. Tully, Chem. Phys. Lett. **12**, 564 (1972); (c) M. Solc, Mol. Phys. **12**, 101 (1967); (d) N. B. Slater, *ibid.* **12**, 107 (1967).
[45]Using a torsional circumference of 10 Å, this translates to a linear velocity of about 4×10^4 cm/s which is consistent with estimates given in Ref. 41.
[46]F. E. Doany, E. J. Heilweil, R. Moore, and R. M. Hochstrasser, J. Chem. Phys. **80**, 201 (1984).
[47]T. J. Majors, U. Even, and J. Jortner **81**, 2330 (1984).
[48](a) N. DeLeon and B. J. Berne, J. Chem. Phys. **75**, 3495 (1981); (b) B. J. Berne, N. DeLeon, and R. O. Rosenberg, J. Phys. Chem. **86**, 2166 (1982).
[49]W. L. Hase, in *Dynamics of Molecular Collisions, Part B*, edited by W. H. Miller (Plenum, New York, 1976), Chap. 3.
[50]G. Varsanyi, *Assignments for Vibrational Spectra of Seven Hundred Benzene Derivatives* (Wiley, New York, 1974).